

JAN 2 1076

14 1976

AEDC-TR-75-150

cy. 2



LASER RAMAN STUDY OF WATER VAPOR

BLOCK ENGINEERING, INC.
19 BLACKSTONE STREET
CAMBRIDGE, MASSACHUSETTS 02139

December 1975

Final Report for Period 22 April 1974 — 21 April 1975

Approved for public release; distribution unlimited.

Approved for public release; distribution unlimited.
2206000-0000

Prepared for

DIRECTORATE OF TECHNOLOGY
ARNOLD ENGINEERING DEVELOPMENT CENTER
AIR FORCE SYSTEMS COMMAND
ARNOLD AIR FORCE STATION, TENNESSEE 37389

NOTICES

When U. S. Government drawings specifications, or other data are used for any purpose other than a definitely related Government procurement operation, the Government thereby incurs no responsibility nor any obligation whatsoever, and the fact that the Government may have formulated, furnished, or in any way supplied the said drawings, specifications, or other data, is not to be regarded by implication or otherwise, or in any manner licensing the holder or any other person or corporation, or conveying any rights or permission to manufacture, use, or sell any patented invention that may in any way be related thereto.

Qualified users may obtain copies of this report from the Defense Documentation Center.

References to named commercial products in this report are not to be considered in any sense as an endorsement of the product by the United States Air Force or the Government.

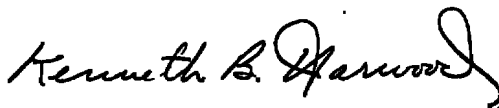
This final report was submitted by Block Engineering, Inc. 19 Blackstone Street, Cambridge, Massachusetts 02139, under contract number F40600-74-C-0013 with Arnold Engineering Development Center, Arnold Air Force Station, Tennessee 37389. Captain Kenneth B. Harwood (CF), Directorate of Technology (DY), was the AEDC technical manager.

This report has been reviewed by the Information Office (OI) and is releasable to the National Technical Information Service (NTIS). At NTIS, it will be available to the general public, including foreign nations.

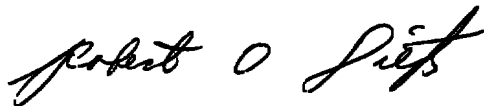
APPROVAL STATEMENT

This technical report has been reviewed and is approved for publication.

FOR THE COMMANDER



KENNETH B. HARWOOD
Captain, CF
Research & Development
Division
Directorate of Technology



ROBERT O. DIETZ
Director of Technology

UNCLASSIFIED

REPORT DOCUMENTATION PAGE		READ INSTRUCTIONS BEFORE COMPLETING FORM
1 REPORT NUMBER AEDC-TR-75-150	2 GOVT ACCESSION NO	3 RECIPIENT'S CATALOG NUMBER
4 TITLE (and Subtitle) LASER RAMAN STUDY OF WATER VAPOR		5 TYPE OF REPORT & PERIOD COVERED Final Report - April 1974 to April 1975
		6 PERFORMING ORG REPORT NUMBER
7 AUTHOR(s) Philip J. Miller, Anthony J. Modestino, and Stanley M. Klainer		8 CONTRACT OR GRANT NUMBER(s) F40600-74-C-0013
9 PERFORMING ORGANIZATION NAME AND ADDRESS Block Engineering, Inc. 19 Blackstone Street Cambridge, Massachusetts 02139		10 PROGRAM ELEMENT, PROJECT, TASK AREA & WORK UNIT NUMBERS Program Element 65807F
11 CONTROLLING OFFICE NAME AND ADDRESS Arnold Engineering Development Center (DYFS), Air Force Systems Command, Arnold Air Force Station, Tennessee 37389		12 REPORT DATE December 1975
		13 NUMBER OF PAGES 109
14 MONITORING AGENCY NAME & ADDRESS (if different from Controlling Office)		15 SECURITY CLASS (of this report) UNCLASSIFIED
		15a DECLASSIFICATION DOWNGRADING SCHEDULE N/A
16 DISTRIBUTION STATEMENT (of this Report) Approved for public release; distribution unlimited.		
17 DISTRIBUTION STATEMENT (of the abstract entered in Block 20, if different from Report)		
18 SUPPLEMENTARY NOTES Available in DDC		
19 KEY WORDS (Continue on reverse side if necessary and identify by block number) <div style="display: flex; justify-content: space-between;"> <div> water vapor Raman scattering Stokes asymmetric top </div> <div> spectral profile temperature specie density flames </div> </div>		
20 ABSTRACT (Continue on reverse side if necessary and identify by block number) Low resolution experimental measurements of the Raman Stokes scattering cross-sections and band shapes of water vapor are presented as a function of temperature. The trace scattering theoretical band profiles are compared satisfactorily to the experimental results. The results indicate that low resolution Raman data of water vapor may be used to obtain temperature and specie density information in flames.		

UNCLASSIFIED

PREFACE

The work in this report was performed under Contract No. F40600-74-C-0013 for the Arnold Engineering Development center, Arnold Air Force Station, Tennessee, 37389, by Block Engineering, Inc., 19 Blackstone Street, Cambridge, Massachusetts, 02139. This report includes all work performed during the contract period 22 April 1974 to April 1975 under Program Element 65807F. The report was submitted on 1 October 1975. The work was performed under the direction of Air Force Technical Manager, Kenneth B. Harwood, Captain (CF), Directorate of Technology, Arnold Air Force Station, Tennessee.

The authors acknowledge the generous help of Dr. Stewart Hemple of Block Engineering, Inc. and Professor Ellis R. Lippincott (deceased) of the University of Maryland in the theoretical portions of this report.

The reproducibles used in the publication of this report were supplied by the authors.

TABLE OF CONTENTS

SECTION		Page
I	INTRODUCTION	
1.0	General	9
1.1	Organization of the Report	9
II	INSTRUMENTATION AND EXPERIMENTAL METHOD	
2.0	General	11
2.1	Raman Spectrometer	11
2.2	Burner Description	12
2.2.1	Porous Plugburner	12
2.2.2	Needle Burner	13
2.3	Description of Thermocouple	18
2.4	Determination of Temperature From the Calculated Raman Spectra of N ₂	21
2.5	Description of Flow Meters	21
2.6	Experimental Procedure	26
III	EXPERIMENTAL DATA	
3.0	General	35
3.1	Spectra	35
3.2	Spectra of Water Vapor Between 1500 and 1750 K	35
3.3	Polarized Raman Spectra of Water Vapor	43
3.4	Raman Cross Section of H ₂ O at Different Wavelengths	45
3.5	Discussion of Experimental Errors	45
IV	THEORETICAL CONSIDERATIONS	
4.0	Calculation of the Rotational/Vibration Spectra of Water Vapor	50
4.1	Pure Vibrational Spectrum	50
4.1.1	The Harmonic Oscillator - Normal Coordinate Vibrational Model	50
4.1.2	The Anharmonic Vibrational Model	55

TABLE OF CONTENTS

SECTION		Page
4.1.3	Resonant Interactions	58
4.1.4	Fermi Resonance	58
4.1.5	The Rotational Bands	63
4.1.5.1	Asymmetric Top Rigid Rotor	63
4.2	Calculation of the Rotation-Vibration Spectra in the ν_1 Region of Water Vapor	67
4.2.1	Higher Order Approximation to the Energies of an Asymmetric Rotor - Artificial Distortion	67
4.2.2	Higher Approximations to the Energies of an Asymmetric Rotor	68
4.2.2.1	Rotation-Vibration Interaction	68
4.3	Coriolis Perturbation	69
4.4	Selection Rules for A-Type Bands in an Asymmetric Top	73
4.5	Calculation of Relative Line Strengths	73
4.6	Calculation of the Band Envelope	74
V	CALCULATED RAMAN BAND PROFILES OF THE ν_1 REGION OF H ₂ O VAPOR	
5.1	Computer Program for Calculation of the Q Branch of H ₂ O Vapor in the ν_1 Region	77
5.1.1	Limitations and Description of Calculations	77
5.1.2	Slit Function	78
5.1.3	Computer	78
5.2	Calculated Spectra at Various Temperatures Relative to 298 K	80
5.3	Vibrational Hot Band Contributions to the Raman Profile	80
5.4	Theoretical Line Analysis	83
5.5	Comparison of Calculated Contours to Observed Contours	88
VI	CONCLUSIONS AND RECOMMENDATIONS	
6.0	Summary of Work Accomplished	92
6.1	Use of H ₂ O Raman Band Profiles for Temperature and Specie Density Studies	93

TABLE OF CONTENTS

		<u>Page</u>
SECTION 6.2	Recommendations for Extended Work	94
6.2.1	Modification of the Computer Program . . .	94
6.2.2	Experimental Work on Other Molecules . . .	94
	REFERENCES	95
	APPENDIX	97

LIST OF ILLUSTRATIONS (continued)

<u>Figure</u>		<u>Page</u>
19	The Raman Spectra of H_2O and N_2 at ~ 1650 K and ~ 1750 K. The Spectra were Obtained with Locked-In Amplifier and Synchronous Detection Electronics. The Excitation Frequency was 4880 \AA with Power Levels of Nearly 8 Watts. The Spectral Slit Width is $\sim 8 \text{ cm}^{-1}$	41
20	The Polarized (Upper Curve) and Depolarized (Lower Curve) Raman Spectra of Water Vapor at ~ 1075 K	44
21	The Geometry of the Water Molecule	51
22	The Normal Vibrations of the Non-Linear XY_2 Molecule	53
23	Asymmetric Energy Levels for Low J	66
24	Comparison of Instrument and Theoretical Slit Functions	79
25	Calculated Raman Band Profiles of H_2O in the ν_1 Region of H_2O Vapor (8 cm^{-1} resolution) at Various Temperatures Relative to 298 K . . .	81
26	The Vibrational Hot Band Components of H_2O	82
27	Calculated H_2O Raman Spectrum with 8 cm^{-1} Resolution	84
28	Calculated Raman Profile of H_2O with 4 cm^{-1} Resolution	85
29	Calculated Raman Band Profile of H_2O with 2 cm^{-1} Resolution	86
30	Comparison of Experimental and Calculated Raman Band Profiles	89
31	Plot of Temperature Versus the Full Width at Half Height of the Experimental and Theoretical Raman Band Contours of H_2O Vapor	90

LIST OF TABLES

<u>Table</u>		<u>Page</u>
1	Monochromator Wavelength Calibration . . .	12
2	Experimental Data Showing Measured Flame Velocity Versus Flame Temperature Data for Constant and Pre-Flame Composition	17
3	Experimental Results for Temperatures Between 1000 and 1500K	42
4	Relative Raman Cross Sections of H ₂ O Vapor	43
5	Vibrational Transitions and Relative Intensities at Various Temperatures in the ν_1 Region	59
6	Ground Vibrational State Rotational Energy Levels for J=0 to 5	60
7	The Constants α_1 for the Water Molecule (cm ⁻¹)	61
8	Rotational Constants for the Ground and General Excited States of Water (cm ⁻¹) . .	61
9	Calculated and Observed Q Branch Transitions Between the Vibrational States (000) and (100) for H ₂ O Vapor	70
10	Partial List of Line Positions	87

SECTION I INTRODUCTION

1.0 GENERAL

This is the Final Report for Contract No. F40600-74-C-0013, with Arnold Engineering Development Center, Arnold Air Force Station, Tennessee. This Contract contains both experimental measurements of the Raman Stokes scattering cross-sections of water vapor as a function of temperature, and a theoretical calculation of the spectral profiles for the asymmetric top model of the water vapor molecule as a function of temperature.

Laser Raman scattering diagnostic techniques are being developed at AEDC for the measurement of concentration, and vibrational, rotational temperatures. This is to be applied to single and multiple gaseous species in both single and multiphase flow fields for flow diagnostic test applications. These fields occur in the exhausts of jet engines and rockets and in combustion chambers. Water vapor is present to some degree as a combustion product in all these applications.

One phase of this program entailed the development of two burners which produced H_2/O_2 and H_2/Air flames. These burners produced steady temperature and flow rate flames. Thus, water molecules in thermal equilibrium were obtained over a sufficiently large area to allow their examination by laser Raman spectroscopy.

1.1 ORGANIZATION OF THE REPORT

This report is divided into two major parts. The first, Sections II and III, describes the experimental apparatus, procedure and results. Section II contains information on the spectrometer, burner design, flow meters, thermocouple data

and the experimental procedure. Section III presents the spectral data and a discussion of the experimental error.

The second part, Sections IV and V, discusses the theoretical considerations and calculations. The results of these calculations are tabulated in Section V. The computer program used in the theoretical calculations can be found in the Appendix.

SECTION II

INSTRUMENTATION AND EXPERIMENTAL METHOD

2.0 GENERAL

This section describes the Raman spectrometer used in acquiring all the spectral measurements presented in this report. It describes the design and development of the burners and the calibration of the flow meters. Discussions are devoted to temperature measurements by thermocouple for determination of temperature gradients in the flame and use of the Raman profile of the N_2 spectrum for obtaining flame temperatures. The experimental procedure is described in detail for the manner in which all measurements were made.

2.1 RAMAN SPECTROMETER

The initial spectral observations are confined to the Stokes bands arising from 4880 Å incident radiation from an argon ion laser (Spectra Physics Model 165) operated for all data at 1.2 watts. The scattered light was analyzed by a double monochromator (Jarrell Ash Model 25-100) with 5000 Å blazed gratings. The detector was a cooled ITT-FW130 photomultiplier operated in the pulse-counting mode with dark count levels of about 5 counts per sec for this work.

The overall experimental arrangement was designed to have the laser beam travelling parallel to the entrance slit (that is, vertically) such that the Raman scattered light is collected 90° to the incident light direction. The Raman scattered light was collected by a lens with focal length 100 mm (F number, 8). The width of the laser beam was about 100 μm. One to one magnification of an image of 1.5 cm in height from the scattering zone area was accepted in the entrance slit

of the monochromator. The slits were set at 350 μm which produced a spectral slit width of about 8.0 cm^{-1} for the wavelength of the scattered light considered.

In following our regular procedure, the Jarrell-Ash Model 25-100 Raman monochromator was aligned for optimum throughput. Initial calibration of the spectrometer was carried out by a representative of Jarrell-Ash. Prior to starting the collection of experimental data we rechecked the calibration of the monochromator. The wavelength of light used and the sources from which they were obtained are listed in Table 1.

TABLE 1
MONOCHROMATOR WAVELENGTH CALIBRATION

<u>Source</u>	<u>λ, Å</u>	<u>Grating Order</u>	<u>cm^{-1}</u>
Hg lamp	4358.3	I	22944.5
	5460.7	I	18312.5
	4046.6	II	12356.2
Argon laser	4579.	I	21839.
	4880.	I	20492.
	5145.	I	19436.

Figure 1 is a plot obtained from this data. Wavenumber difference (difference between true wavenumber and absolute wavenumber reading on monochromator) is plotted against true wavenumber of the source.

2.2 BURNER DESCRIPTION

2.2.1 Porous Plugburner

The flames studied in the 1000 to 1500 K range were produced by a water-cooled sintered brass porous ($\sim 50 \mu\text{m}$)

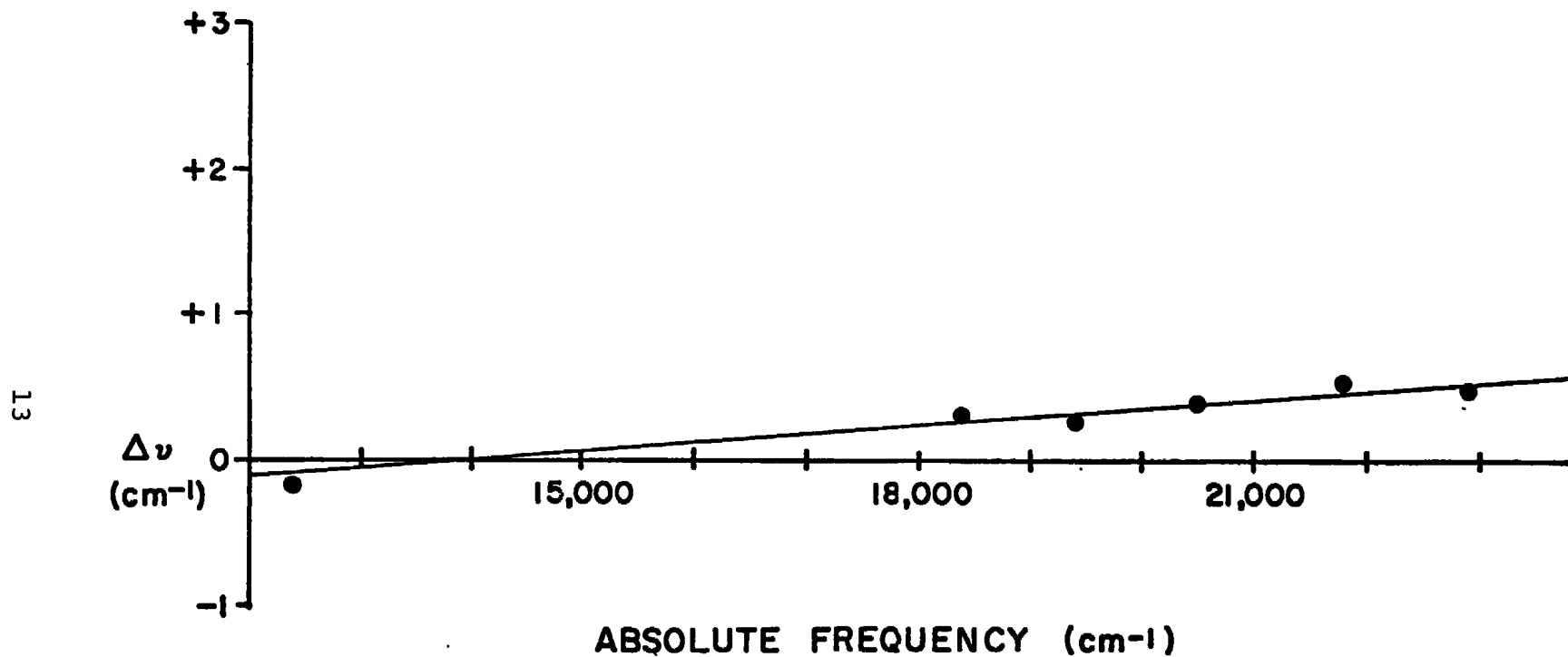


FIGURE 1
MONOCHROMATOR WAVELENGTH CALIBRATION

plug burner (diameter, 2.5 cm). It was operated horizontally and burned into another water-cooled porous plug placed about 2 cm away which, in turn, was connected to a rough vacuum line. In this fashion, a stable horizontal flame at atmospheric pressure was produced. There are several advantages to this type of burner: (1) the laminar flame is fairly uniform over a rather large area offering an ideal scattering test zone, (2) the outer layers of the flame have been shown to serve as a shield to inhibit atmospheric contamination of the inner flame which will be studied. The burner is shown in Figure 2. Contained in Figure 3 is a top view of the burner setup.

An excellent description and study of this burner design can be found in the literature on combustion.⁽¹⁾ The main advantage of this burner is that it is possible to cool a flame to a lower temperature than that which would result from adiabatic combustion. The resulting flames are very stable and extremely flat - independent of the size of the burner. The previous studies⁽¹⁾ of this burner have also demonstrated that flame temperature can be varied approximately 200 K by merely changing the pre-flame gas flow rate and keeping the gas constituents constant. See Table 2 for some results on H_2 , O_2 , and N_2 flames.

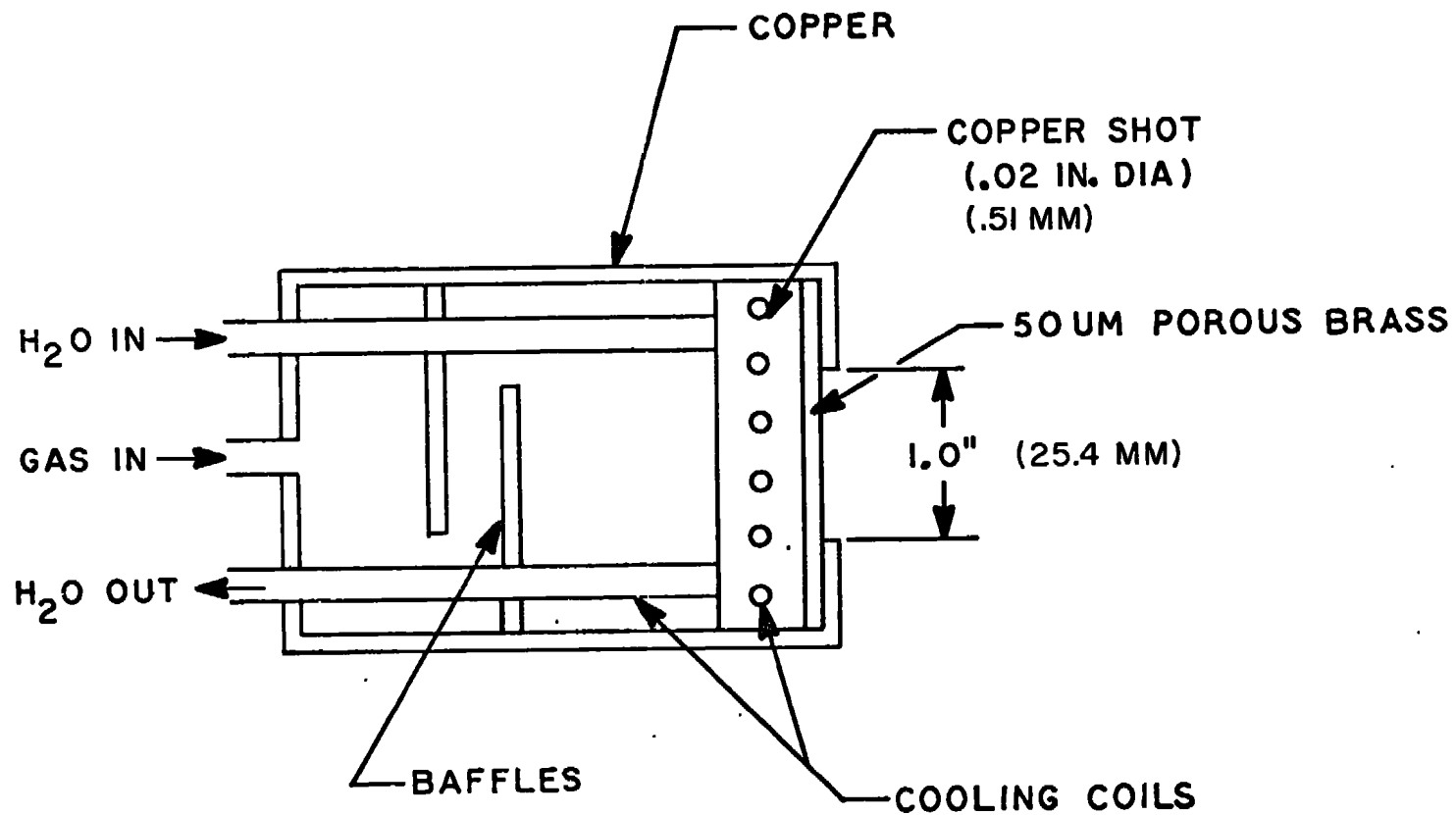


FIGURE 2
DIAGRAM OF COOLED POROUS METAL BURNER

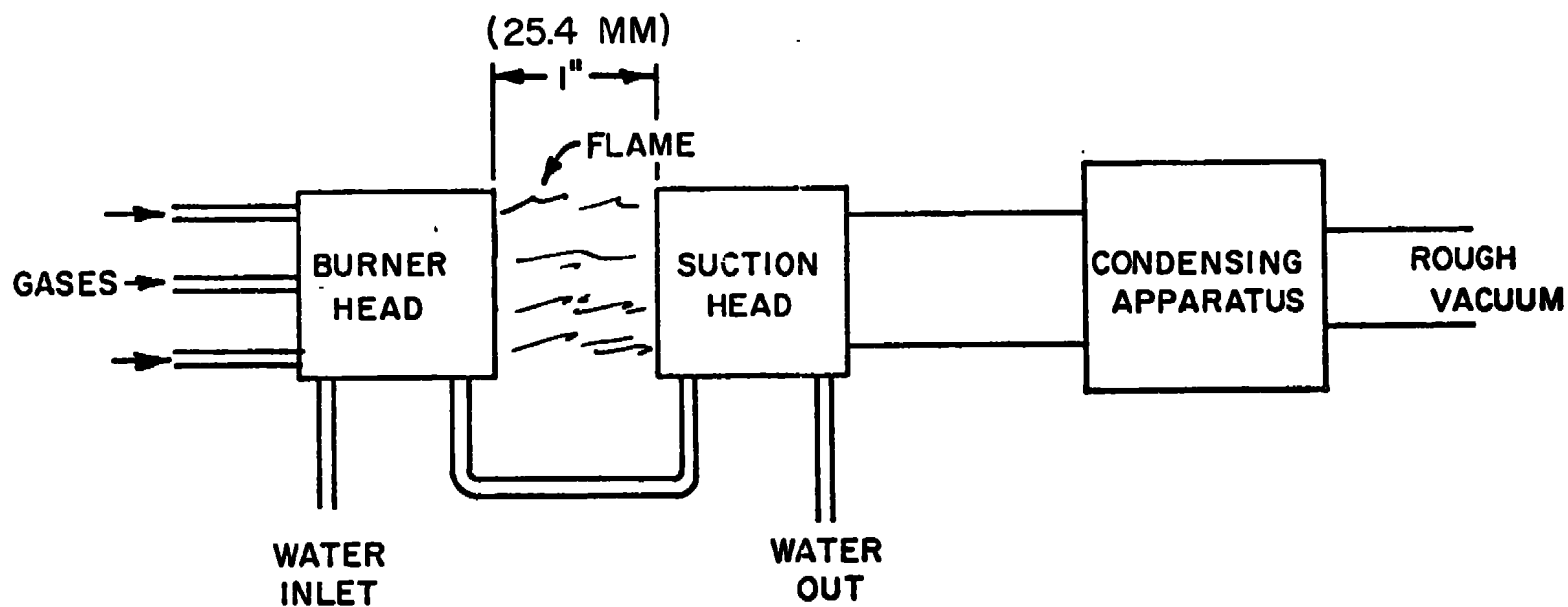


FIGURE 3
BURNER SET UP

TABLE 2

EXPERIMENTAL DATA SHOWING MEASURED FLAME VELOCITY VERSUS
FLAME TEMPERATURE DATA FOR CONSTANT AND PRE-FLAME COMPOSITION**

Flame 1, 2H_2 : 5N_2 : 10O_2

<u>Velocity* (ml/s)</u>	<u>Temperature (K)</u>
59.0	1550
98.5	1667
173.0	1818

Flame 2, 1.2H_2 : 5N_2 : 10O_2

<u>Velocity (ml/s)</u>	<u>Temperature (K)</u>
49.2	1409
108.0	1540
197.0	1667

* Velocities are evaluated for the total pre-flame compositions at the stated molar ratio at 25°C and 1 atmos. pressure.

** Data collected by W. E. Kaskan (Ref. 1).

2.2.2 Needle Burner

Due to the characteristics of the flame produced by the porous plug burner, it was necessary to construct another burner in order to obtain reasonably good data at temperatures higher than 1500 K. The water-cooled, metal, porous plate burner produces a higher temperature only in the flames tip and only over a very small region which is not satisfactory for obtaining good Raman spectra. The alternate burner is constructed from 400 stainless-steel hypodermic tubes tightly soldered together. The internal diameter of the tubes is 0.045 cm. This gives primary cones not more than 1/2 mm in height, and an excellent laminar flame. The experimental flame is about 2 cm in diameter. The specific design is after that of Padley and Sugden⁽²⁾. The burner is water cooled and premixes the gases. The burner easily obtains temperatures between 1500 K and 2500 K. Experimental studies have shown that the flame's central portion is well shielded up to 10 cm away from the burner head. This burner is shown schematically in Figure 4.

2.3 DESCRIPTION OF THERMOCOUPLE

The thermocouple was prepared from platinum and platinum-13% rhodium wire of 0.0005 inches (0.0127 mm) in diameter. The thermocouple junction was butt welded. The wire is contained in ceramic insulating tubes. The junction is supported above the insulating tube such that only the thermocouple wire is in the flame area. Low velocity and low temperature H₂-air flames are known to produce very little, if any, catalytic heating at the platinum thermocouple's surface⁽¹⁾, so it will not be necessary to coat the thermocouple with fused quartz or ceramic materials to eliminate this effect.

TUBE BURNER

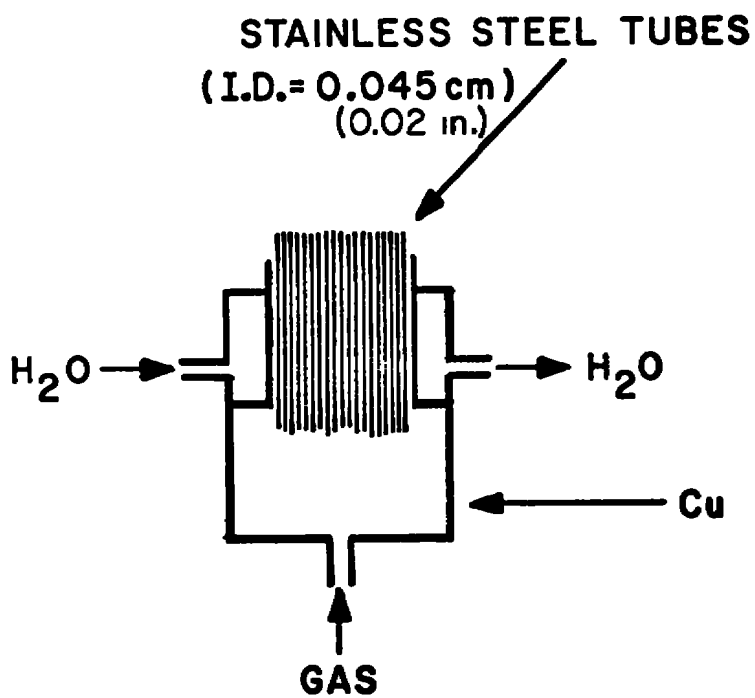


FIGURE 4
TUBE BURNER

Kaskan⁽¹⁾ has shown that corrections for radiation cooling caused by the thermocouple wire are significant and may be calculated from

$$\Delta T_{\text{rad}} = \frac{1.25 \epsilon \sigma T_w^4 D^{0.75}}{\lambda} \frac{\eta}{\rho v}^{0.25} \quad (2-1)$$

where

- ϵ is the thermocouple emissivity,
- σ is the Stefan-Boltzmann constant,
- T_w is the wire temperature,
- D is the wire diameter,
- λ is the thermal conductivity of the gas at T_w ,
- η is the viscosity of gas at T_w , and
- ρv is the mass flux, gm/sec/cm².

Estimates of ΔT_{rad} were obtained using the values of the parameters in equation (2-1) as given by Kaskan⁽¹⁾ for temperatures between 1000 K and 1800 K. The results, however crude, are comparable with those of Lapp⁽³⁾ and are given below.

Measured Temperature	Correction Due to ΔT_{rad}
1000 K	18 K
1200 K	30 K
1400 K	40 K
1600 K	50 K
1800 K	65 K

2.4 DETERMINATION OF TEMPERATURE FROM THE CALCULATED RAMAN SPECTRA OF N_2

In Figure 5 is a series of calculated Raman spectra of the vibrational Stokes scattering of N_2 at various temperatures showing the intensity dependence on temperature of the first vibrational hot band. The calculations are similar to those previously described in the literature⁽³⁾. Plotted in Figure 6 is the ratio of the areas of the N_2 fundamental and its hot band versus temperature. By using the observed relative intensities of N_2 , the vibrational temperatures of N_2 can be found from the curve. As will be observed, these temperatures agree remarkably well with those of the corrected thermocouple measurements and they probably have the same accuracy of ± 30 to 40 K. Use of a thermocouple is definitely required in order to insure that the Raman scattering zones utilized contain only small temperature gradients.

2.5 DESCRIPTION OF FLOWMETERS

The flowmeters used in this study are commercially available Roger Gilmont Flowmeters. The models used consisted of two size number 3 and one size number 2. Size number 3 has a useful range of 200 to 1,200 ml/min of air. The number 3 flowmeters were used to monitor the H_2 and N_2 flowrates. The number 2 flowmeter was used for the O_2 flowrate.

In Figure 7 is shown a comparison of a volume displacement calibration curve and a calculated curve. The calculations are based on a method supplied by the manufacturer. The experimental and calculated curves agree very well.

In Figure 8 are volume displacement calibration curves comparing two different flowmeters of the same type. Agreement

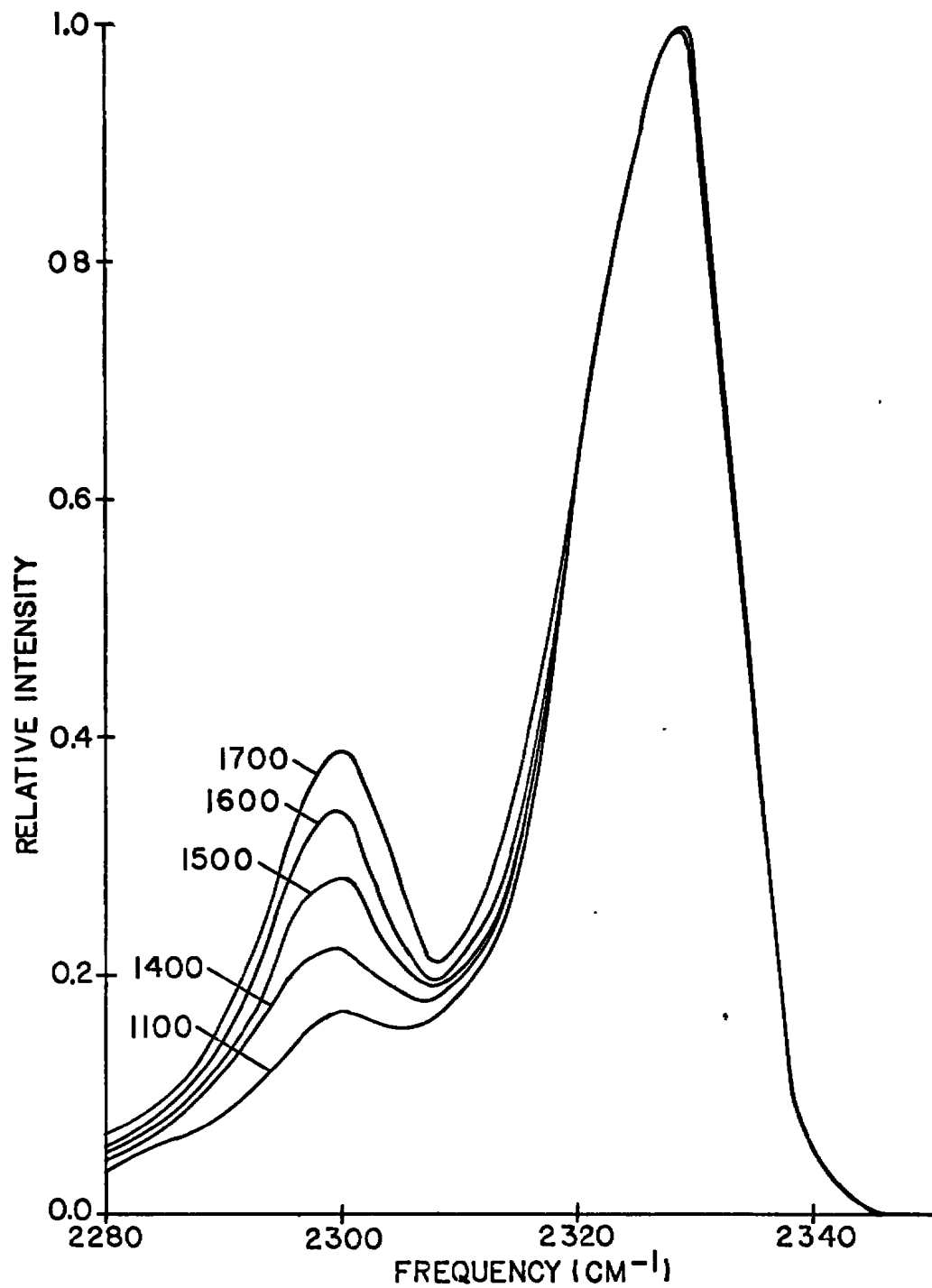


FIGURE 5
CALCULATED N_2 SPECTRUM AT VARIOUS TEMPERATURES (DEGREES K)

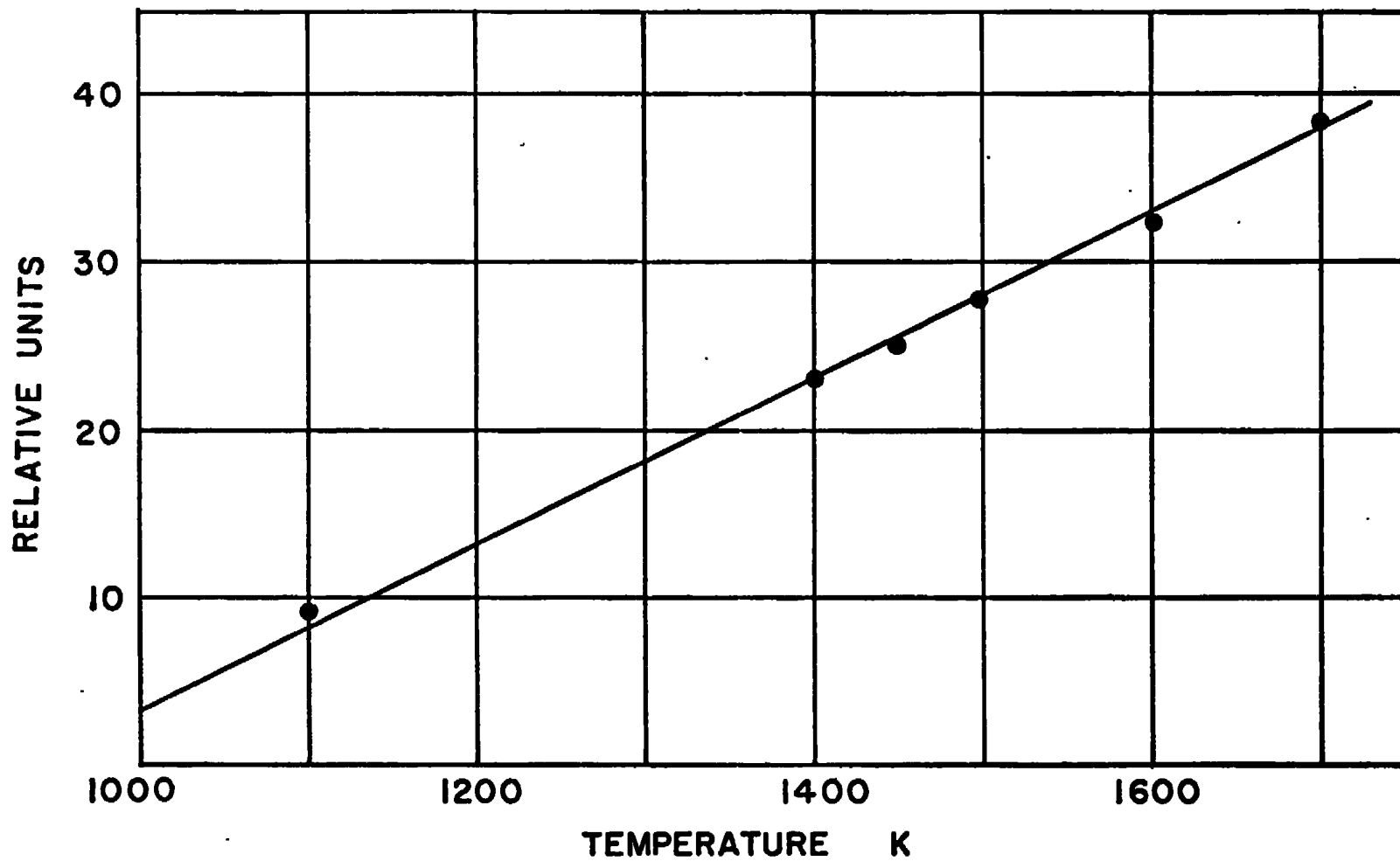


FIGURE 6
PLOT OF RELATIVE INTENSITIES
OF 1st AND 2nd VIBRATIONAL STATES OF NITROGEN VERSUS TEMPERATURE

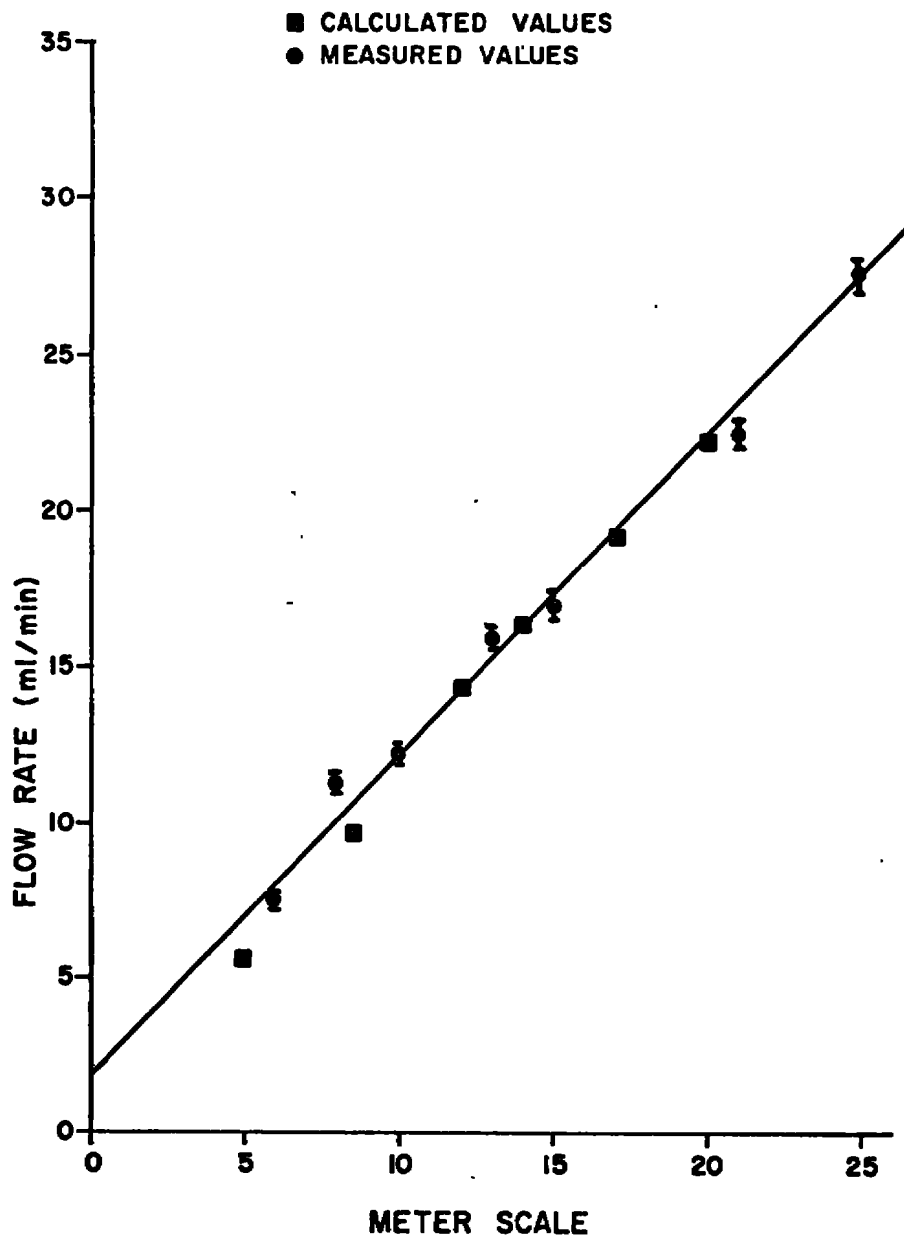


FIGURE 7
CALIBRATION OF FLOWMETERS

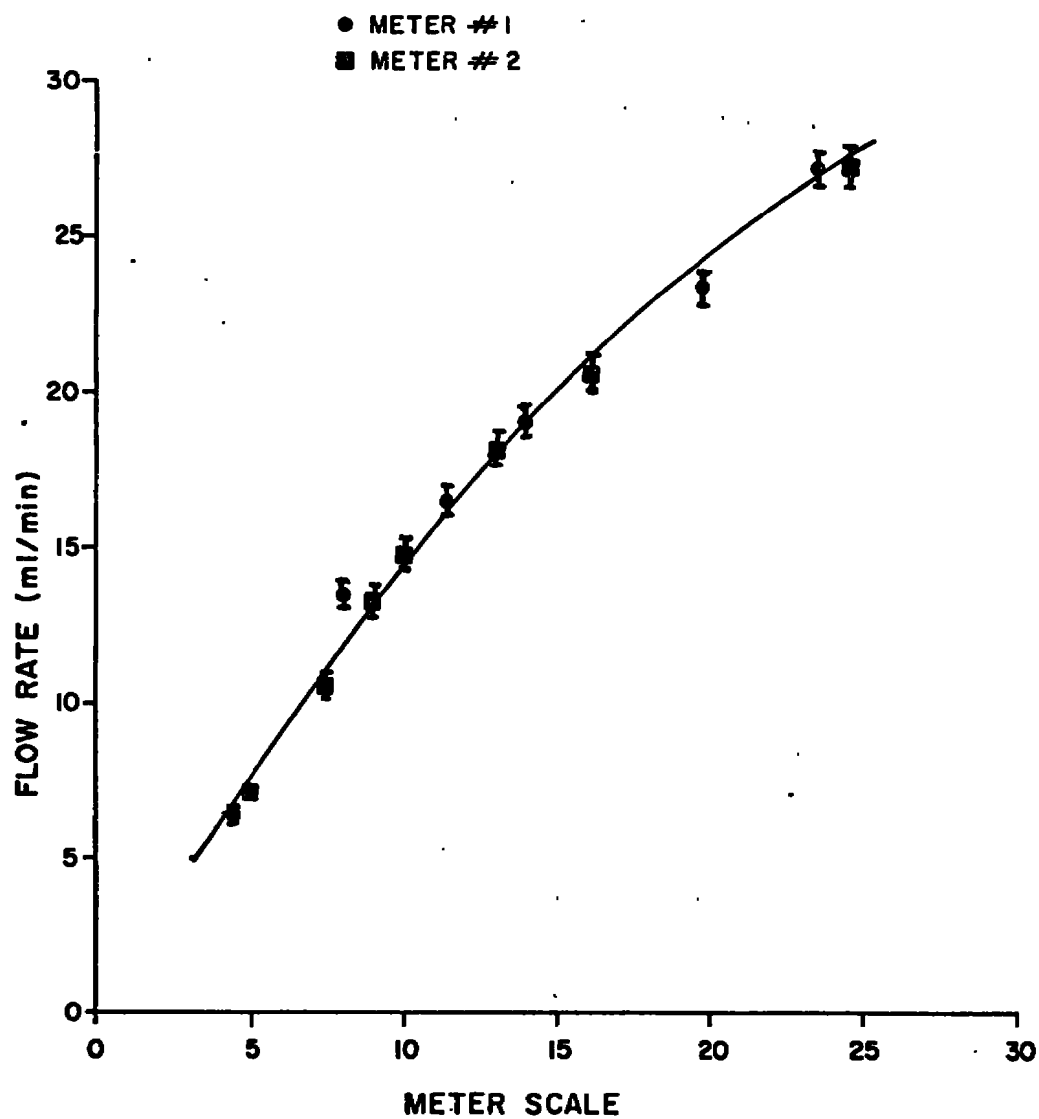


FIGURE 8
COMPARISON OF 2 FLOWMETERS CALIBRATIONS

here is very good, indicating reproducibility in the manufacturing of the flowmeters. Water was the liquid used in the volume displacement experiments and the appropriate corrections for the vapor pressure of H_2O and the solubility of the gases in water have been applied to the results.

Because of the good agreement between the theory and experimental results and in order to avoid experimental errors, calculated calibration curves were used for determining flow rates. Presented in Figures 9, 10 and 11 are experimental calibration curves for H_2 , N_2 and O_2 respectively.

2.6 EXPERIMENTAL PROCEDURE

The first step in obtaining any spectral data consisted of accurately aligning the laser beam and burner with respect to the slits. Also included in this process is the accurate mapping of the flame as a function of temperature. Since the thermocouple was used as an indicator of the foregoing prerequisites, it was necessary to mount it on a precisely calibrated x-y-z translator. This, in turn, was mounted on the optical rail. A low power laser beam was then turned on and the usual alignment procedure was carried out to position the beam parallel to the slits. The center of the thermocouple wire was then aligned with the laser beam, so that a vertical path of the thermocouple was parallel to the entrance slit.

The laser beam was then blocked off and the burner ignited. The flame was adjusted to the approximate temperature to be investigated. Vertical measurements of temperature were taken about every 2 mm to define the center of the flame.

Next, by manipulation of the height of the burner and repetitive temperature measurements, the center of the flame

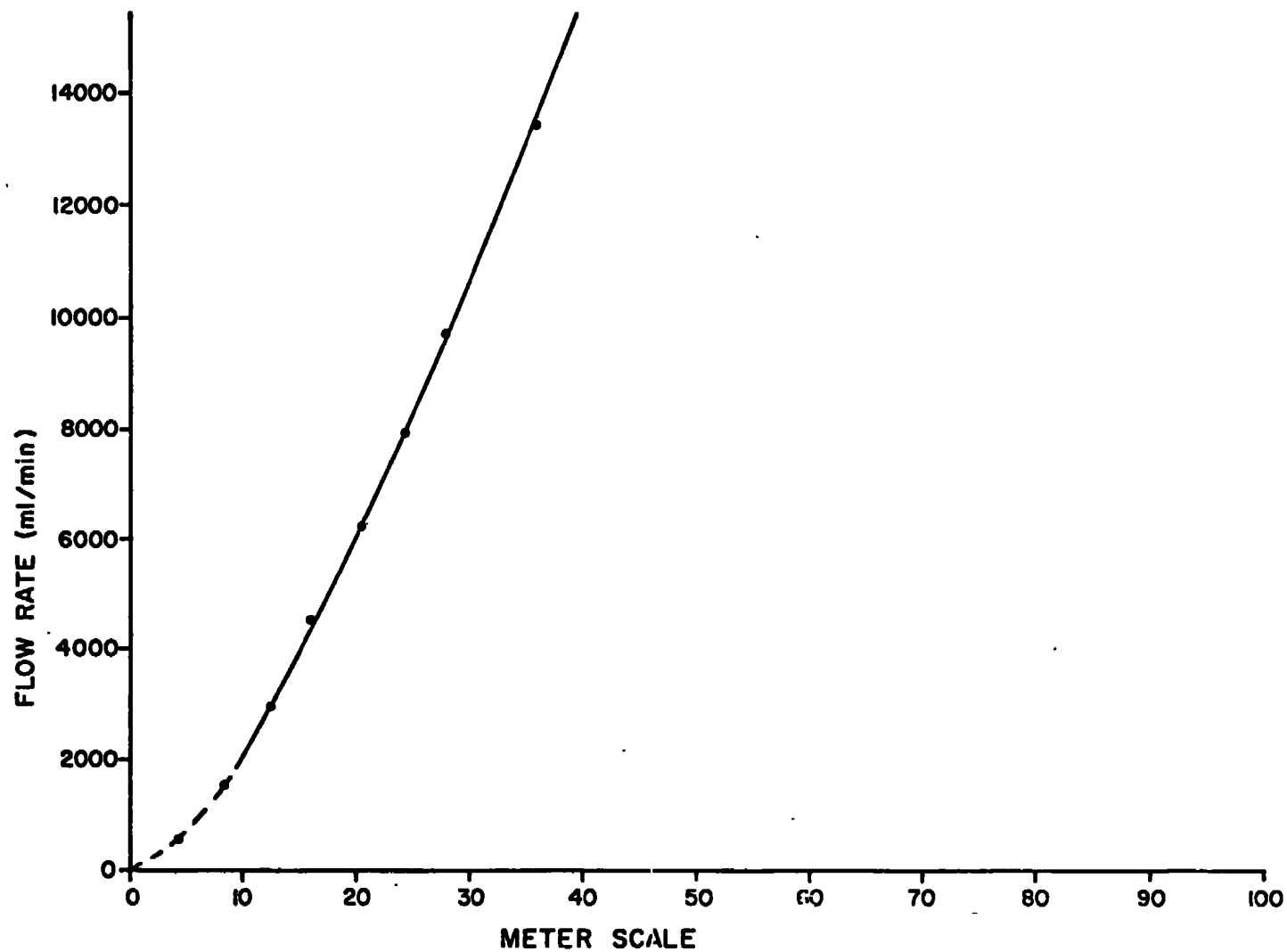


FIGURE 9
CALIBRATION OF H₂ FLOWMETER

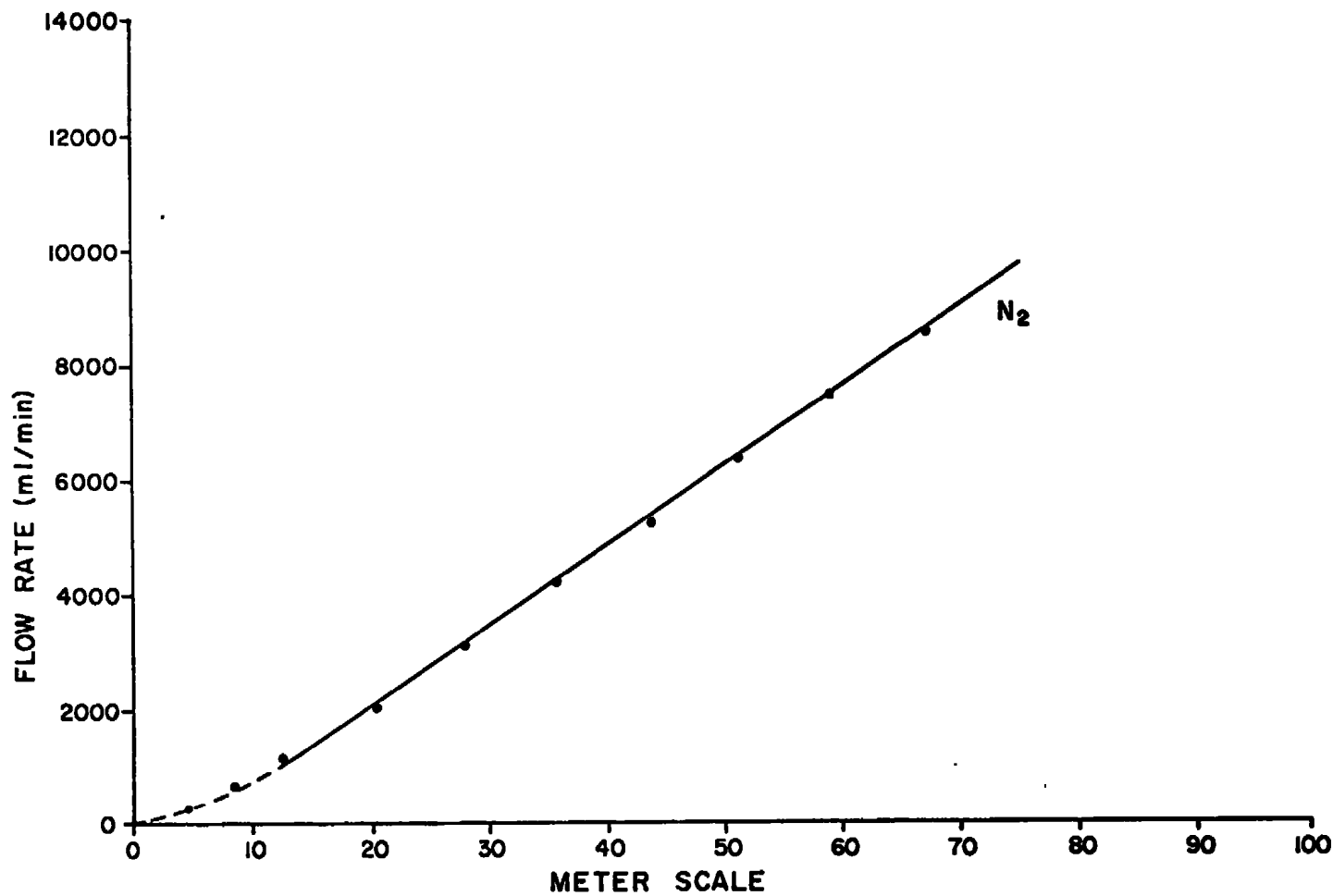


FIGURE 10
CALIBRATION OF N₂ FLOWMETER

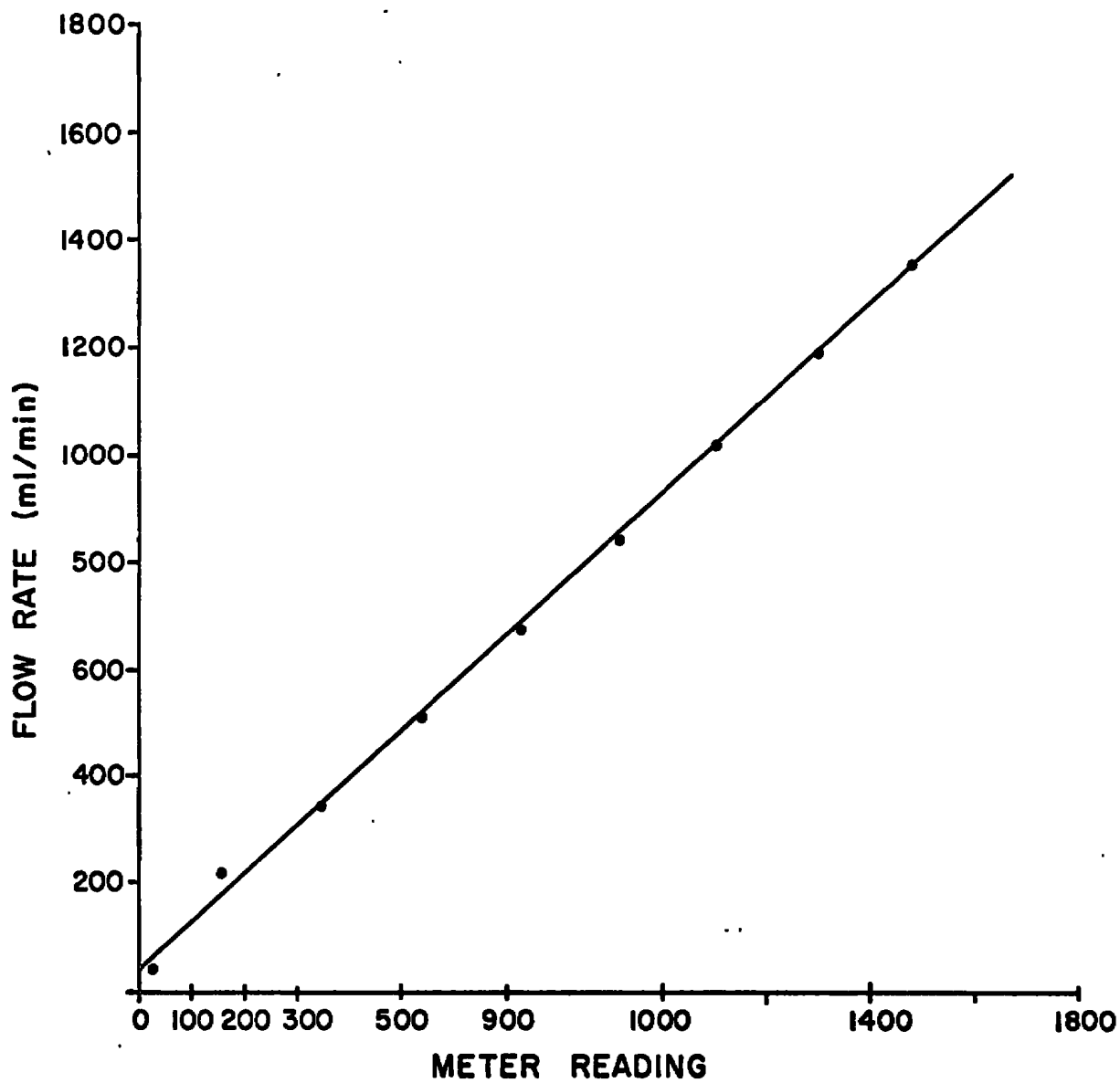


FIGURE 11
CALIBRATION OF O₂ FLOWMETER

was aligned with the center of the slit. Parallelism and alignment was again rechecked by use of a low power laser beam.

The burner was then turned off, the thermocouple lowered out of the optical path and the spectra of the nitrogen and water vapor content of the laboratory atmosphere were obtained. This was carried out primarily as a final check on instrument throughput. Typical spectra of this type are shown in Figures 12 and 13 respectively. The radiative background for the spectra is about 20 cps.

Without disturbing anything, the flame was then reignited and adjusted to the appropriate temperature. The parallelism and alignment of the thermocouple with respect to the slits and laser beam was checked again. The flame was then mapped by measuring the temperature at 1 mm intervals, for a distance of 5 mm, on each side of the center of the flame. The slit heights were then closed to a height of 10 mm. A low power laser beam was allowed once more to shine on the thermocouple and the image followed on the slits to insure that the temperature limits to be investigated fell within the allowed slit height, and that those not desired were blocked off.

A typical example for further discussion would be that of the 1500 K flame. Here, the measured temperature of the flame in the area where Raman scattered light was collected varied from a maximum of 1550 K at the center to as low as 1425 K at the outer edges of the measured zone. Several reasons can exist for these variations. Cold air is possibly mixing with the less dense hot flame gases to cause the flame to break down and/or there is a large inhomogenous flame produced from irregular surface pores causing an uneven flow of the gases. Before obtaining accurate Raman cross-sections

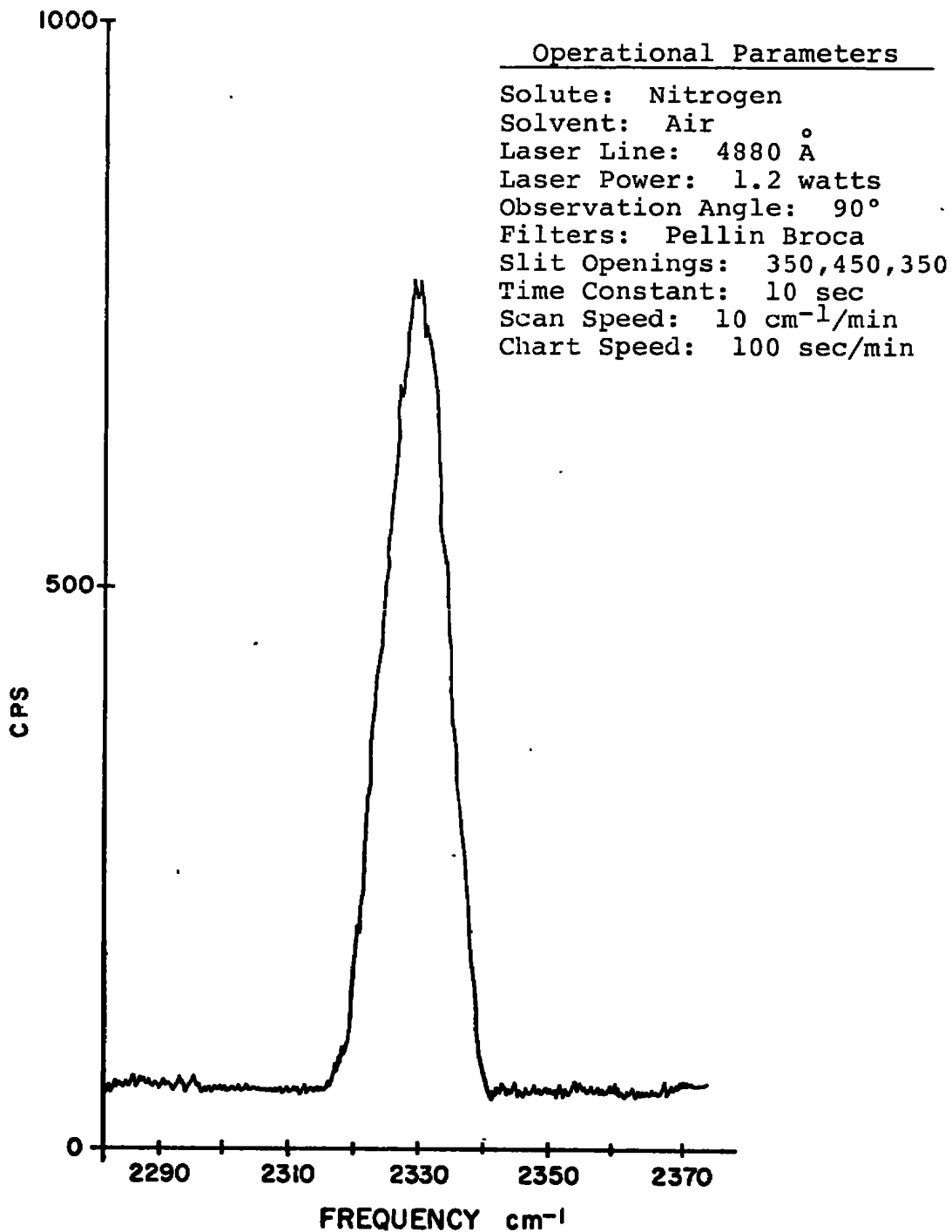


FIGURE 12
ROOM TEMPERATURE RAMAN SPECTRUM OF N₂
IN LABORATORY ATMOSPHERE

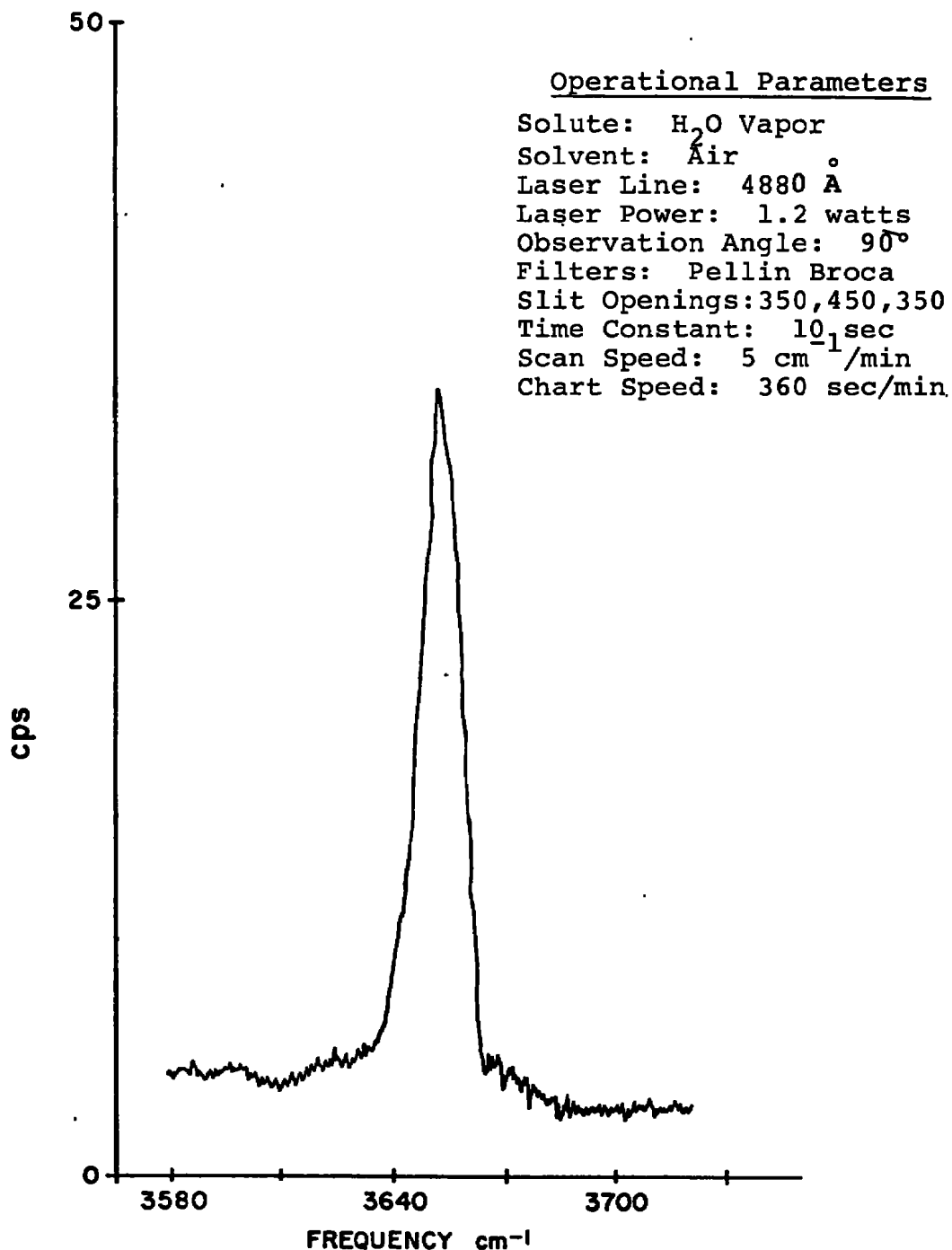


FIGURE 13
ROOM TEMPERATURE RAMAN SPECTRUM OF H₂O VAPOR
IN LABORATORY ATMOSPHERE

of water vapor in various flames, it is necessary to completely characterize the flames across the burner surface. Previous studies⁽³⁾ of flames produced with similar burners have shown that it was necessary, in order to obtain a homogenous temperature region in the flame, to collect scattered light from only a 5 mm section of the flame. Also, increasing the mass flow of the flame will produce a more stable flame with less atmospheric influence. Previous studies⁽¹⁾ have also shown that by placing a steel screen immediately above the burner a much flatter and more homogenous flame can be produced.

It is quite evident in the spectral data obtained, even at room temperature, that asymmetry exists in the vibrational bands of water vapor. This asymmetry is observed to increase sharply in the 1500 K flame. The half-band width of the water band at room temperature approximately doubles at the higher temperature and the maximum peak position decreases in energy from $\sim 3652 \text{ cm}^{-1}$ to $\sim 3646 \text{ cm}^{-1}$. A shoulder on the low energy side of the band, (an $\sim 15 \text{ cm}^{-1}$ shift) also is observed to appear at the high temperature. The low energy asymmetry is produced by the fact that all the $\Delta J = 0$ rotational lines corresponding to the Q branch do not overlap each other exactly. There is a progressive shift to lower energies caused by the vibrational-rotational interaction. The fine structure on the band has been qualitatively assigned by Lapp et. al.⁽⁴⁾ to be due to a large population of an excited vibrational state, $v = 1$, whose transition is observed at lower energy due to anharmonic effects. It is obvious from these spectra that the temperature dependence of the water vapor band will not be as large as that of N_2 and H_2 which have been previously investigated in flames^(3, 4). The ultimate sensitivity

of calculated band contours in comparison to experimentally obtained data is undoubtedly limited by the quality of the experimental data.

All areas or intensities obtained both for cross section calculations and temperature measurements were determined by use of a planimeter. They represent, in most cases, an average value of ten determinations on each spectrum.

SECTION III

EXPERIMENTAL DATA

3.0 GENERAL

Presented in this section are the high temperature experimental Raman spectra of H_2O vapor. All the spectra were obtained using the 4880 Å laser line except where cross section scaling was carried out using the 5145 Å line. A discussion of the experimental error is also included in this section.

3.1 SPECTRA

The experimental apparatus and procedure have been described in Section 2.5. In Figure 14 are shown traces of spectra of water vapor and nitrogen at various temperatures demonstrating their temperature dependence. The spectra were obtained by locating in the flames, with the aid of a thermocouple, fairly homogeneous temperature regions. The slit height was adjusted so that only Raman scattered light from that region was collected.

Included in Table 3 are the calculated Relative Raman cross sections of water vapor relative to nitrogen for 90° scattering. The individual spectra of H_2O and N_2 at the various temperatures, as described in Table 3, are shown in Figures 15 through 18 respectively.

3.2 SPECTRA OF WATER VAPOR BETWEEN 1500 K AND 1750 K

The spectra of water vapor and N_2 at approximately 1650 K and 1750 K are shown in Figure 19. The temperatures were determined from the N_2 band profiles. Thermocouple data at these temperatures is unreliable due to an excess of radiation cooling and catalytic effects. Above 1500 K, the burners which

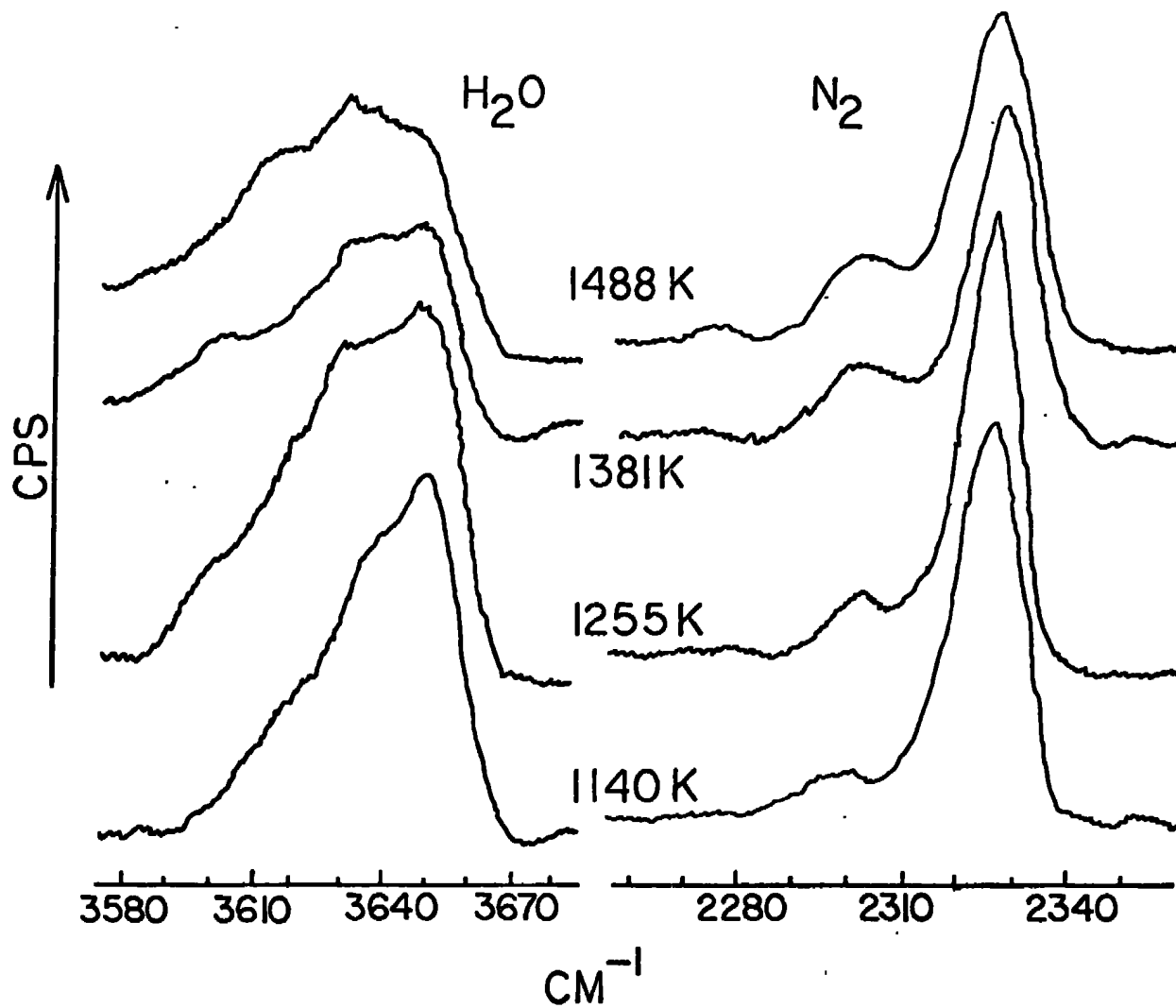


FIGURE 14
SPECTRA OF H₂O AND N₂ AT VARIOUS TEMPERATURES

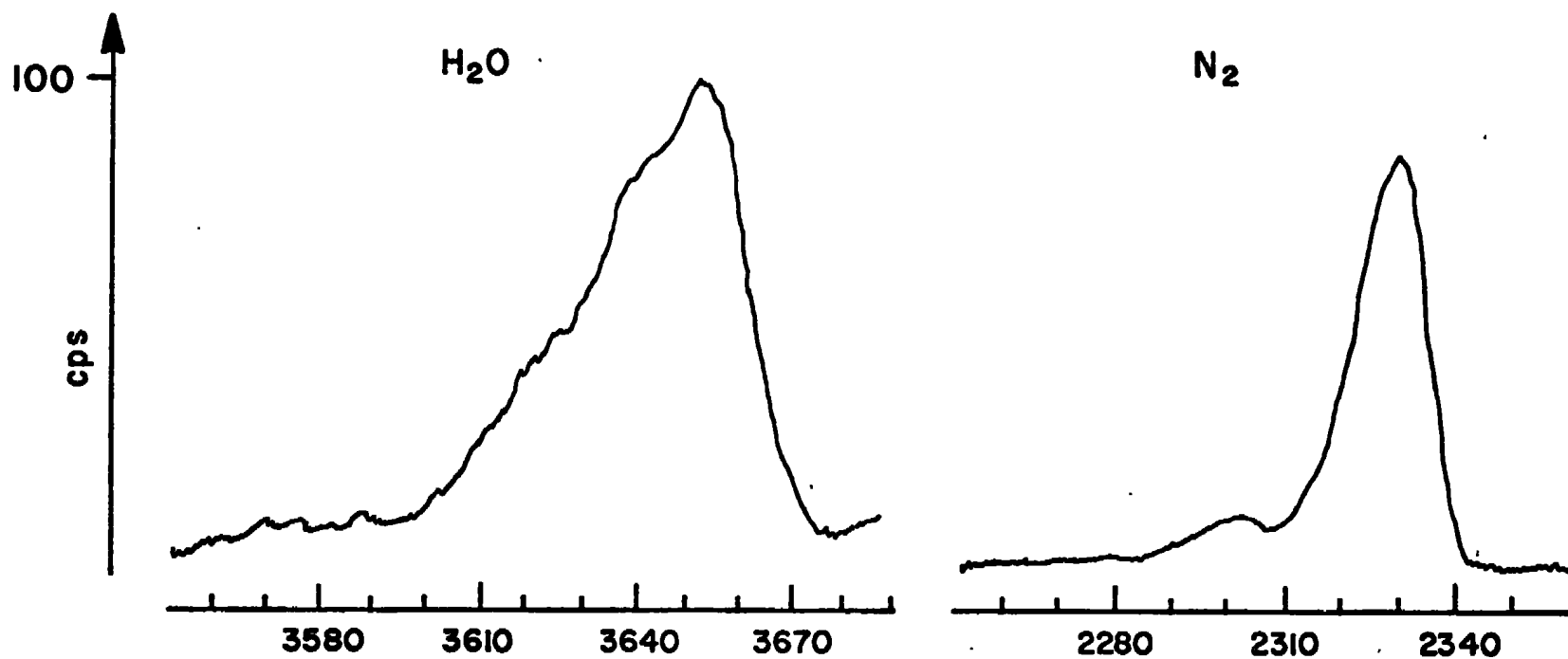


FIGURE 15
SPECTRA OF H_2O AND N_2 AT 1140 K (SLIT WIDTH 8 cm^{-1} , 4880 Å)

1255 K

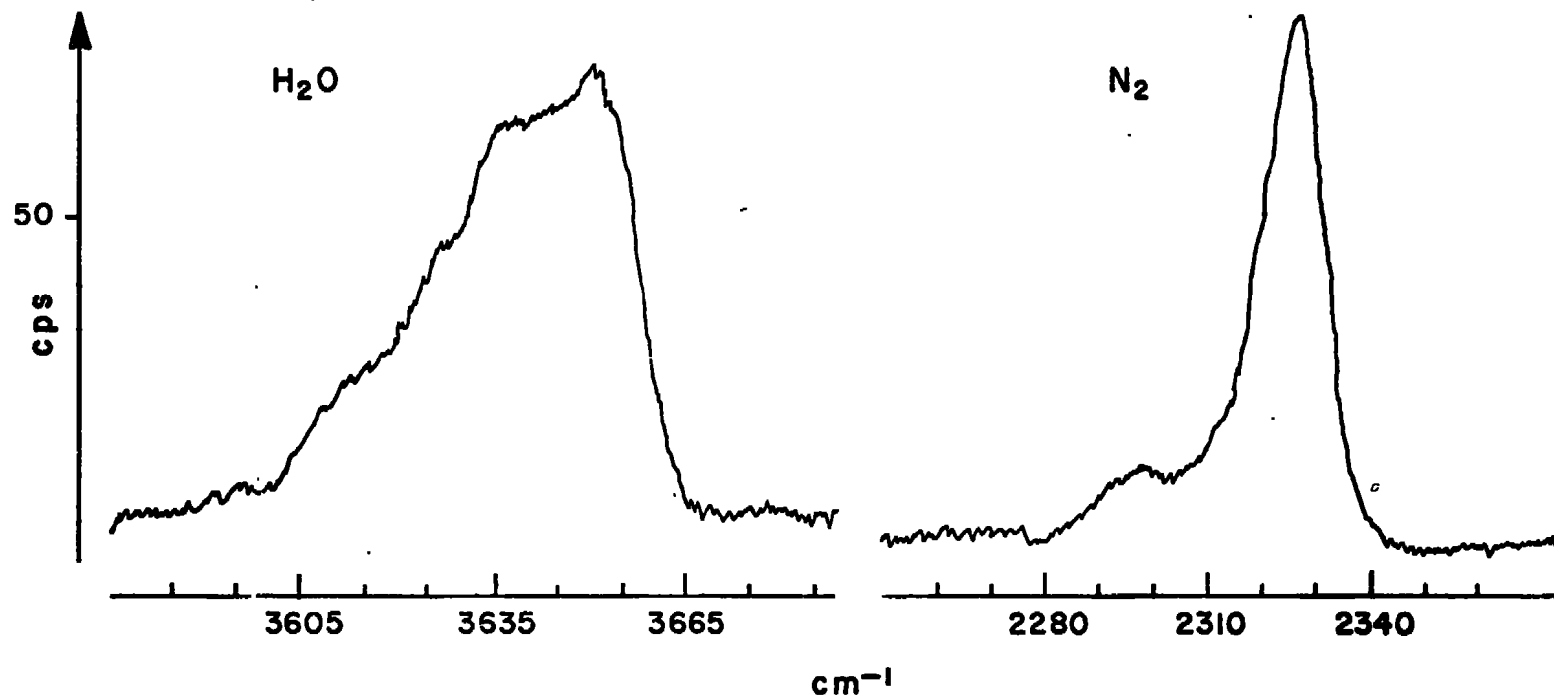


FIGURE 16

SPECTRA OF H₂O AND N₂ AT 1255 K (SLIT WIDTH 8 CM⁻¹, 4880 Å)

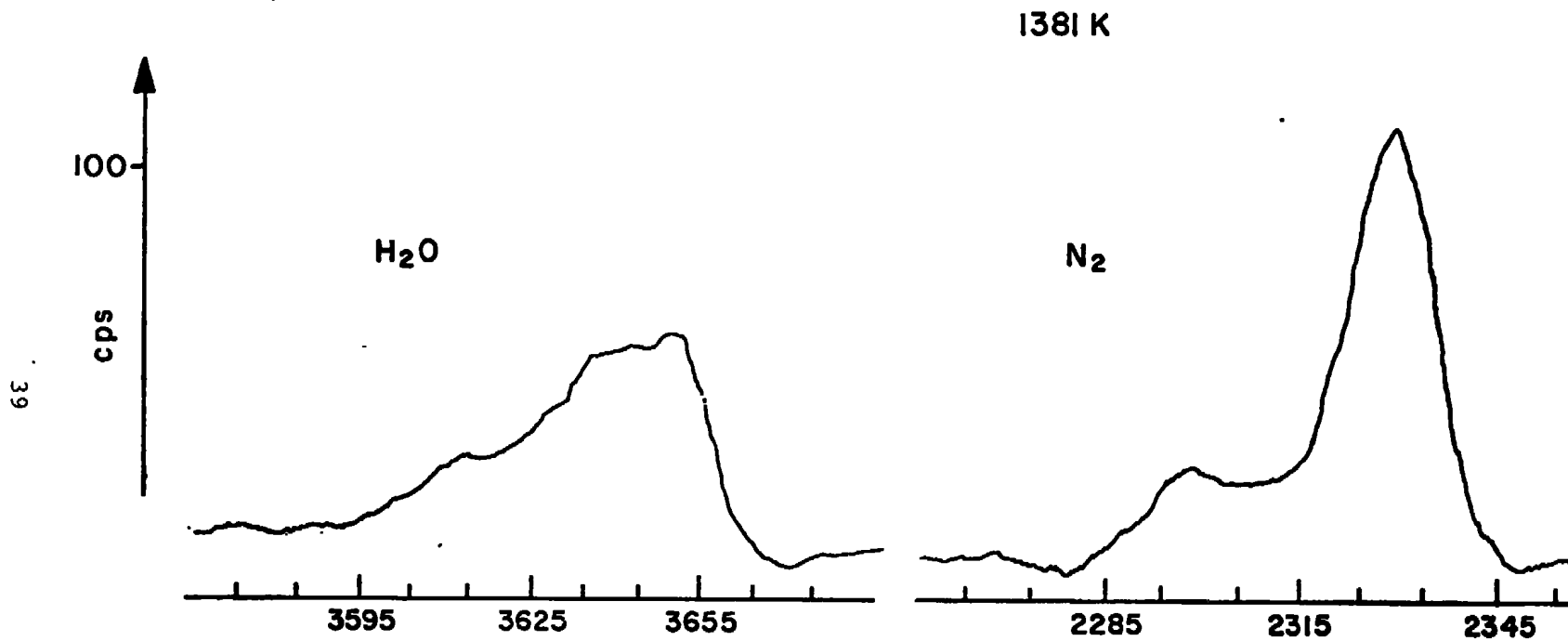


FIGURE 17
SPECTRA OF H₂O AND N₂ AT 1381 K (SLIT WIDTH 8 CM⁻¹, 4880 Å)

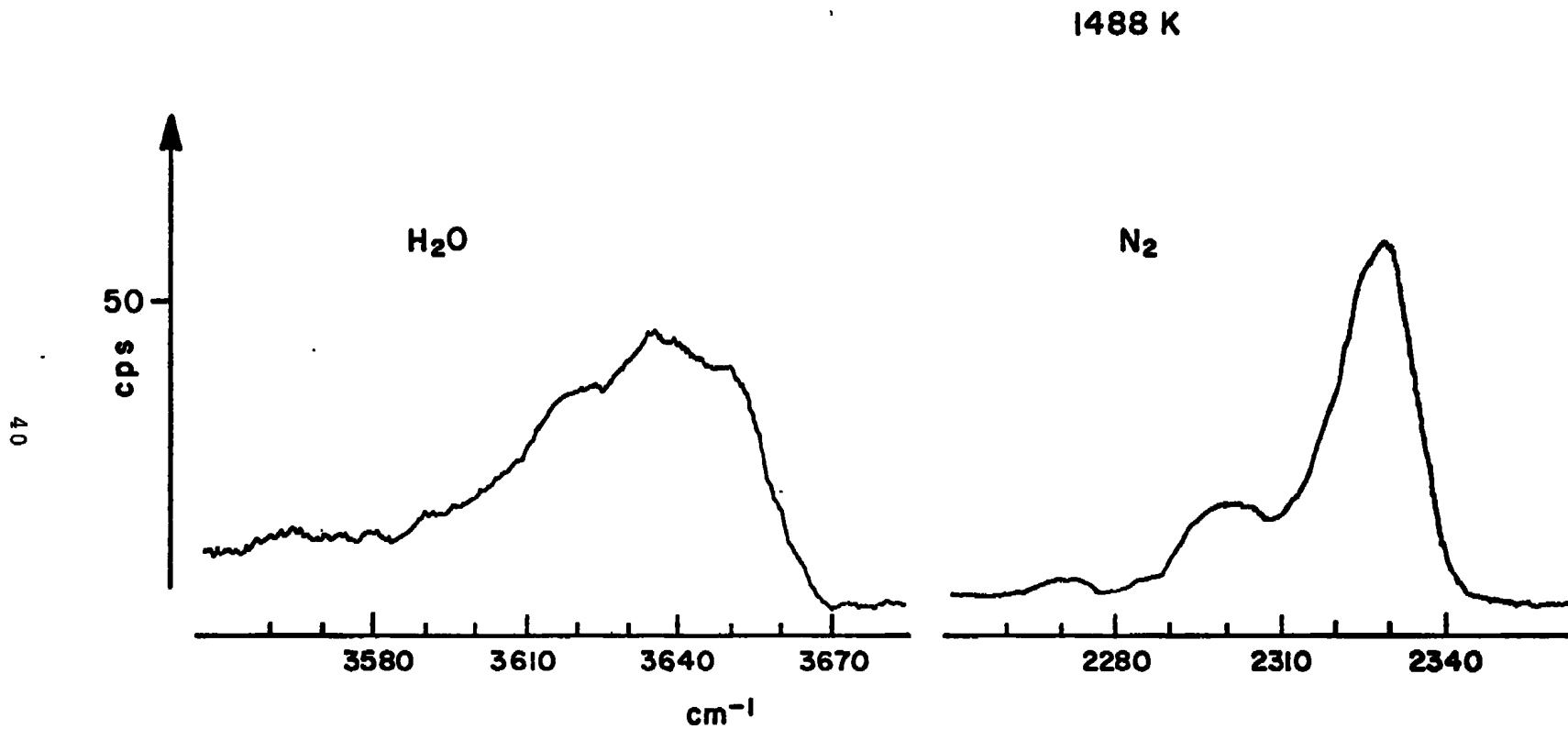


FIGURE 18
SPECTRA OF H_2O AND N_2 AT 1488 K, (SLIT WIDTH 8 cm^{-1} , 4880 \AA)

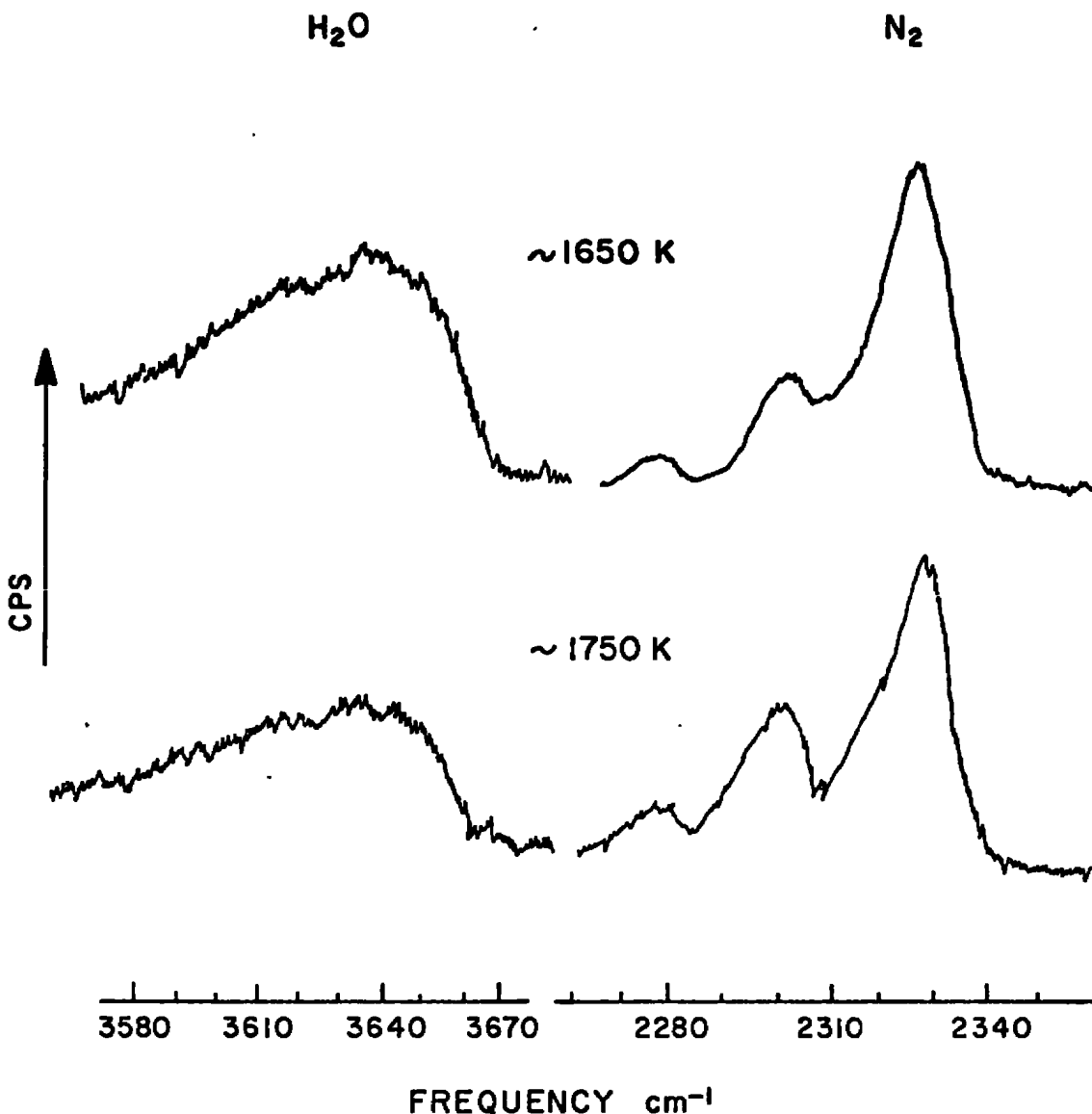


FIGURE 19

THE RAMAN SPECTRA OF H_2O AND N_2 AT $\sim 1650 K$. AND
 $\sim 1750 K$. THE SPECTRA WERE OBTAINED WITH LOCKED-IN
AMPLIFIER AND SYNCHRONOUS DETECTION ELECTRONICS.
THE EXCITATION FREQUENCY WAS 4880 \AA WITH POWER
LEVELS OF NEARLY 8 WATTS. THE SPECTRAL SLIT WIDTH
IS $\sim 8 \text{ cm}^{-1}$

TABLE 3
EXPERIMENTAL RESULTS FOR TEMPERATURES BETWEEN 1000 AND 1500K

Calculated* Temperature	Average Thermocouple + Temperature (Range)	Flow Rates (l/m)			Slit Heights	90° Relative Raman Cross Sections H ₂ O/N ₂
		H ₂	O ₂	N ₂		
1100 K	1107 (1080→1145)	2.150	1.510	4.675	10 mm	2.47
1255 K	1241 (1239→1252)	1.0	0.5	2.3	11.4	2.2
1381 K	1413 (1376→1440)	0.5	0.25	0.3	12.7	2.5
1488 K	1500 (1408→1605)	0.5	0.25	2.0	8.9	2.9

* Temperature estimated from calculated N₂ spectra.

+ Corrected for radiation cooling.

we employed caused significant Na emission to result in the flame gases, thereby making it impossible to use the photon counting detection electronics. To eliminate the flame emission signals from the Raman signals, we utilized a technique which is often used to remove infrared emission interferences from infrared absorption spectral data. The technique involves chopping the source, in our case the laser beam, and using synchronous detection of the Raman signal. The method, in effect, subtracts the emission spectral data from the observed Raman plus emission signals. The method does have one disadvantage in that considerably more noise is added to the final spectrum. With our present experimental apparatus, however, this was the only way we could obtain data. Table 4 gives the temperatures and flow rates of the pre-flame gases and the calculated relative Raman cross sections for this data.

TABLE 4. RELATIVE RAMAN CROSS SECTIONS OF H_2O VAPOR

Temperature (K)	Flow Rates (l/m)			Raman Cross Section Relative to N_2 For 90° Scattering of 4880 Å
	N_2	H_2	O_2	
1650	7.3	3.3	1.3	2.7
1750	7.3	3.4	1.7	2.6

3.3 POLARIZED RAMAN SPECTRA OF WATER VAPOR

The polarized and depolarized Raman spectra of H_2O vapor at approximately 1075 K were obtained (Figure 20) by placing a polarizer between the monochromator and the sampling area and

$\text{H}_2\text{O (GAS)}$
 $\sim 1075 \text{ K}$

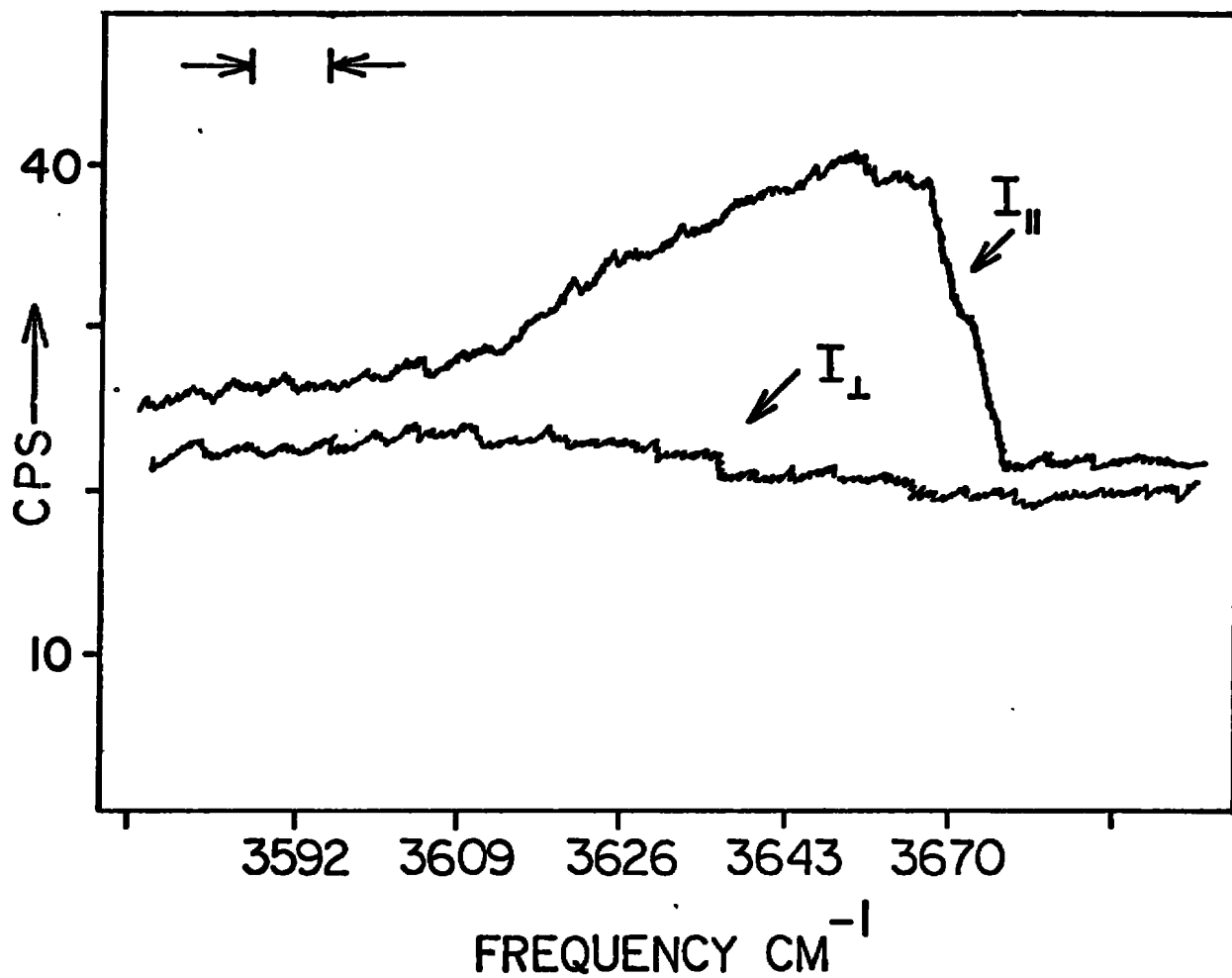


FIGURE 20

THE POLARIZED (UPPER CURVE) AND DEPOLARIZED (LOWER CURVE) RAMAN SPECTRA OF WATER VAPOR AT $\sim 1075 \text{ K}$.

analyzing the Raman scattered light. A polarization scrambler was placed immediately in front of the entrance slit of the monochromator to minimize the effect of the instruments selective sensitivity to polarization. The spectra demonstrated that the Raman scattering of water vapor is essentially polarized and results primarily from the trace of the polarizability tensor.

This greatly simplifies the theoretical calculations as this means that only the Q branch of the rotation-vibration manifold need be considered. This will be discussed in more detail in section 4.6 of this report.

3.4 RAMAN CROSS SECTION OF H_2O AT DIFFERENT WAVELENGTHS

Listed below are temperature Relative Raman cross sections of $\text{H}_2\text{-O}_2\text{-N}_2$ flames using the 5145 Å and 4880 Å exciting lines. The flame temperature gradients were mapped by use of the thermocouple as in obtaining the previous data. The same set up and procedure were used as in obtaining data at 4880 Å. An estimate of the temperature was also obtained using the ratio of the N_2 areas. There appear to be no differences within experimental errors in the Raman cross sections of H_2O between 5145 Å and 4880 Å.

Temperature	Relative Raman Cross Section	
	4880 Å	5145 Å
1107 K	2.47	2.55
1488 K	2.90	2.70

3.5 DISCUSSION OF EXPERIMENTAL ERRORS

There are no significant errors in determination of areas under bands introduced by chart paper linearity, monochromator and chart scan speed. Errors which arise from the response of

the chart pen to spectral events were minimized by scanning the monochromator at rates much slower than those of the response of the system monochromator and chart recorder. The uncertainty in the determination of areas under the Raman profiles arises because of the use of a planimeter. The areas and their relative standard deviation for 10 typical measurements are:

$$A_{\text{H}_2\text{O}} = 2565 \pm 5.94 \text{ cps.cm}^{-1}$$

$$A_{\text{N}_2} = 2255 \pm 48.5 \text{ cps.cm}^{-1}$$

In the present study, a maximum of 2% uncertainty was introduced into the intensity determination by measuring actual areas.

The errors in the number densities of the species of the flame combustion products are introduced by the flow rate and temperature inhomogeneities, and determination techniques. The imprecision of the manufacturer's calibration of the flow meters is 2%, or 1 division, whichever is greater. This calibration was confirmed by our experimental calibration. An example of the uncertainties introduced by the flow rate determinations follows:

The flow rates of the preflame gases for the 1082 K flame were:

$$\text{H}_2 - 2.150 \text{ l/m} \pm 2\%$$

$$\text{N}_2 - 4.675 \text{ l/m} \pm 2\%$$

$$\text{O}_2 - 1.510 \text{ l/m} \pm 2\%$$

Since for the reaction $\text{H}_2 + 1/2 \text{O}_2 = \text{H}_2\text{O}$, O_2 is in excess, the amount of H_2O produced is $2.150 \text{ l/m} \pm 2\%$ and the combustion products of the flame are:

$$\text{H}_2\text{O} - 2.150 \text{ l/m} \pm 2\%$$

$$\text{O}_2 - 0.435 \text{ l/m} \pm 2\%$$

$$\text{N}_2 - 4.675 \text{ l/m} \pm 2\%$$

The error in the total number of moles present in the burnt flame can be estimated by taking the square root of the sum of the squares of the individual gas uncertainties or

$$S = \sqrt{(.043)^2 + (.0935)^2 + (.0302)^2}$$

$$S = 0.10 \text{ l/m}$$

The relative deviation, then, is the uncertainty divided by the total number of moles present, or

$$\text{Relative Deviation} = \frac{0.10}{7.260} = .014 \text{ or } 1.4\%$$

The error in obtaining the mole fractions of the reaction products ($\chi_{\text{H}_2\text{O}}$ and χ_{N_2}) used in calculating the Raman cross section is obtained from their relative deviations and from the deviations of the total number of moles present.

$$\text{Rel. Dev. } (\text{H}_2\text{O}) = 2.5\%$$

$$\text{Rel. Dev. } (\text{N}_2) = 2.5\%$$

Due to the signal to noise statistics of the spectrum, there will also be systematic errors introduced in determining the areas of the Raman bands. In the worst case the S/N ratio is 20. This introduces an error of at least 5% of the total area. The maximum estimated error for determining area ratios then arises from the total estimated error in each area that is to be ratioed.

Thus, the maximum error introduced into the relative density determinations of H_2O to N_2 from flow rate and area data is:

$$\text{Rel.Dev. (MAX)} = \sqrt{2(5\%)^2 + 2(2.5\%)^2} = 8\%.$$

This error estimation does not include instability effects or inhomogeneities within the flame.

The determination of temperature from a ratio of the peak intensities of the N_2 profile introduces not only this error but also errors due to the deconvolution of the N_2 peaks. The error in the determination of the temperature from the Raman nitrogen spectra is a minimum of 10% which does not include gradient effects.

The Raman cross section is given by

$$\sigma_{\text{Raman}} = \frac{\left(A_{H_2O} \right) \left(\kappa_{N_2} \right)}{\left(A_{N_2} \right) \left(\kappa_{H_2O} \right)}$$

The standard relative deviation for σ_{Raman} estimated from the errors due to all sources described above is

$$\text{Rel.Dev. } (\sigma_{\text{Raman}}) = \sqrt{(8)^2 + 2(2.5)^2} = 9\%$$

The errors in the estimated temperatures and number densities which arise from the inhomogeneities in the flame gases, such as density and temperature gradients, are extremely difficult to estimate. Use of a thermocouple to find gases in the flame with the smallest temperature gradients minimized the temperature errors, and use of burner designs which produced excellent flame

sources minimized the density fluctuation errors. Since the temperature measurements and cross section data are obtained from ratios of band areas, these errors are further minimized. They are not completely cancelled, however, since the effects of temperature and density gradients, which primarily smear out the band, are not necessarily the same on different Raman bands.

SECTION IV

THEORETICAL CONSIDERATIONS

4.0 CALCULATION OF THE ROTATIONAL/VIBRATION SPECTRA OF WATER VAPOR

4.1 PURE VIBRATIONAL SPECTRUM

4.1.1 The Harmonic Oscillator - Normal Coordinate Vibrational Model

The equilibrium geometry of water is shown in Figure 21. Water, a non-linear symmetrical XY_2 molecule, has symmetry C_{2v} . Its elements of symmetry are C_2 axis through the O atom and bisecting a line between the H atoms (z-axis), a plane of symmetry σ_{xz} is determined by the three nuclei, and a plane of symmetry σ_{xy} containing the C_2 axis is perpendicular to the σ_{xz} . Non-linear XY_2 molecules have two normal vibrations of species A_1 (ν_1 and ν_2) and one of species B_1 (ν_3). ν_1 and ν_3 are the symmetric and anti-symmetric OH stretches and ν_2 is the bending mode.

From high resolution infrared, far infrared and microwave spectroscopy, the constants of water molecules have been accurately determined. The fundamental vibrations are

$$\begin{aligned}\sigma_1 &= 3651.7 \text{ cm}^{-1} \\ \sigma_2 &= 1595.0 \text{ cm}^{-1} \\ \sigma_3 &= 3755.8 \text{ cm}^{-1}\end{aligned}\tag{4-1}$$

The potential energy of a harmonic XY_2 molecule is

$$2V = K_1(\Delta r_1^2 + \Delta r_2^2) + K_\delta \delta^2\tag{4-2}$$

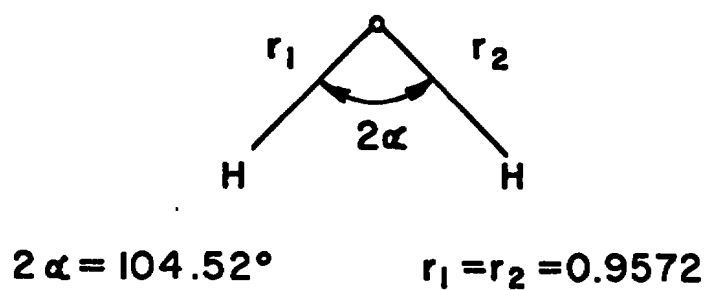


FIGURE 21
THE GEOMETRY OF THE WATER MOLECULE

where

$\Delta r_1, \Delta r_2$ are the changes of X-Y distances,

δ is the change in the apex angle 2α (Figure 21),

K_1 and K_δ are the valence force constants.

The equations for the normal frequencies in terms of the geometry and force constants are as follows:

$$\lambda_3 = 4\pi v_3^2 = (U_Y + 2U_X \sin^2 \alpha) K_1 \quad (4-3)$$

$$\begin{aligned} \lambda_1 + \lambda_2 &= 4\pi^2 (v_1^2 + v_2^2) \\ &= (U_Y + U_X \cos^2 \alpha) K_1 + \\ &\quad 2(U_Y + 2U_X \sin^2 \alpha) K_\delta / \ell^2 \end{aligned} \quad (4-4)$$

$$\lambda_1 \lambda_2 = 16\pi^4 v_1^2 v_2^2 = 2U_Y (U_Y + 2U_X) K_1 K_\delta / \ell^2 \quad (4-5)$$

where U_i is the reciprocal atomic mass.

From equations (4-3), (4-4), and (4-5) and the observed fundamentals,

$$K_1 = 7.76 \text{ mdyne/\AA}^\circ$$

$$K_\delta / \ell^2 = 0.69 \text{ mdyne/\AA}^\circ$$

are determined.

The vibrational motions shown in Figure 22 are the normal coordinates Q_i in terms of which the potential energy, equation (4-2), becomes

$$2V = \sum_{i=1}^3 \lambda_i Q_i^2 \quad (4-6)$$

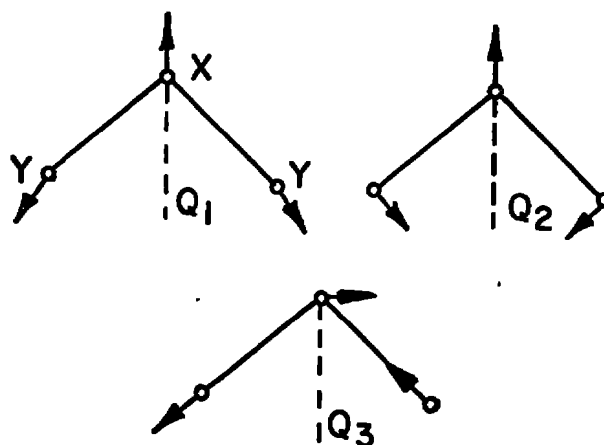


FIGURE 22
THE NORMAL VIBRATIONS OF THE NON-LINEAR XY_2 MOLECULE

This approximation in polyatomic molecules involves two separate assumptions. First, the complicated Lissajous' motion of the vibrating nuclei can be divided into simple motions where each nucleus is moving in a straight line through its equilibrium position. And second, these motions are harmonic oscillations. The normal coordinates shown in equation (4-6) are related to the internal coordinates, q_i , shown in equation (4-2) by a linear transformation, i.e.

$$q_i = \sum_{K=1}^3 l_{iK} Q_K \quad (4-7)$$

Only the internal force constants K_i , shown in equations (4-3), (4-4), and (4-5), have real meaning since they depend on the local bonding. They can be transferred from one molecule to another where identical or even similar bonding situations occur, and they are the basis for characteristic vibrational frequencies.

For a harmonic oscillator, the energy values are given by

$$E_i = h\nu_i (n_i + 1/2), \quad n_i = 0, 1, 2, \dots \quad (4-8)$$

where

$$\nu_i = \frac{1}{2\pi} \sqrt{\lambda_i}$$

The total vibrational energy for triatomic molecules is

$$\begin{aligned} G(n_1, n_2, n_3) &= \frac{E}{hc} = \sigma_1 (n_1 + 1/2) + \sigma_2 (n_2 + 1/2) \\ &\quad + \sigma_3 (n_3 + 1/2) \end{aligned} \quad (4-9)$$

where

$$\sigma_i = \nu_i / C$$

are the classical vibrational frequencies measured in cm^{-1} units. The vibrational quantum numbers are n_1, n_2, n_3 .

4.1.2 The Anharmonic Vibrational Model

When the cubic and quatric terms are considered, the potential energy equation in normal coordinates becomes

$$2V = \sum_i^3 \lambda_i Q_i^2 + \sum_i^3 \sum_j^3 \sum_K^3 \alpha_{ijk} Q_i Q_j Q_K + \sum_i^3 \sum_j^3 \sum_K^3 \sum_\ell^3 B_{ijkl} Q_i Q_j Q_K Q_\ell \quad (4-10)$$

Equation (4-9), the vibration energy equation for a non-linear triatomic molecule, becomes

$$\begin{aligned} G(n_1, n_2, n_3) = & \omega_1(n_1 + 1/2) + \omega_2(n_2 + 1/2) \\ & + \omega_3(n_3 + 1/2) + x_{11}(n_1 + 1/2)^2 \\ & + x_{22}(n_2 + 1/2)^2 + x_{33}(n_3 + 1/2)^2 \\ & + x_{12}(n_1 + 1/2)(n_2 + 1/2) \\ & + x_{13}(n_1 + 1/2)(n_3 + 1/2) \\ & + x_{23}(n_2 + 1/2)(n_3 + 1/2) \end{aligned} \quad (4-11)$$

The ω_i are the frequencies for infinitesimal amplitudes or zero-order frequencies and were first approximated by the σ_i in equation (4-9). The X_{iK} are the anharmonicity constants. The X_{ii} like the $\omega_e X_e$ used for diatomic molecules are a measure of the anharmonicity but the X_{iK} ($i \neq K$) are a measure of the interaction between the vibrations. When the fundamental ν_1 is excited the energy of vibration is

$$\begin{aligned}\sigma_1 &= G(1,0,0) - G(0,0,0) \\ &= \omega_1 + 2X_{11} + 1/2X_{12} + 1/2X_{13}\end{aligned}\quad (4-12)$$

An interpretation of equation (4-12) is that when ν_1 is excited most of the energy stimulates an anharmonic motion Q_1 but a small amount of it also stimulates the motions Q_2 and Q_3 (see Figure 22).

The constants for H_2O are (all in cm^{-1}):

$$\begin{array}{lll}\omega_1 = 3825.32 & X_{11} = -43.89 & X_{12} = -20.02 \\ \omega_2 = 1653.91 & X_{22} = -19.5 & X_{13} = -155.06 \\ \omega_3 = 3935.59 & X_{33} = -46.37 & X_{23} = -19.81\end{array}\quad (4-13)$$

There is a very large interaction (155 cm^{-1}) between the symmetric and antisymmetric stretching vibrations. Comparing σ_i (observed band centers) with ω_i (the zero-order frequencies) a measure of the anharmonicity of the vibrations is derived.

Let

$$U_i = \left(\frac{\sigma_i - \omega_i}{\omega_i} \right) 100 \quad (4-14)$$

then

<u>i</u>	<u>U_i</u>	
1	4.5%	
2	3.6%	
3	4.6%	(4-15)

With equation (4-11) and the constants shown in equation (4-13), we can use energy levels for all excited states and, by differences between them, calculate the observable vibrational transitions. The selection rule for both infrared and Raman transitions in non-linear XY_2 molecules is $\Delta n_i = +1$. This is a harmonic oscillator approximation rule, but since the vibrations are more than 95% harmonic it is relatively accurate. At temperatures well above room temperature, the equilibrium population of excited states (energy levels) will be significant. Vibrational bands in which the initial state is other than the ground vibration state are known as difference bands whose frequency will vary from the fundamental by the relative anharmonicity of the involved states. These bands will have the general formula

$$\sigma_h = G(n_1 + 1, n_2, n_3) - G(n_1, n_2, n_3) \quad (4-16)$$

Since the anharmonicity is small, the transition probability of these bands will be identical to that of the fundamental. Thus, the intensity ratio of a difference band to the fundamental is very nearly equal to Boltzmann factor, $\exp[-(h\nu_i/kT)]$, which gives the relative population of the states at a given temperature. The relative intensities of the hot band to the fundamental for the ν_1 region are shown in Table 5. In the

Raman spectrum of water vapor, only the fundamental should be seen at temperatures below 1000 K; from 1000 K to 2000 K a second line centered 20 cm^{-1} red shifted from the fundamental should be clearly visible. Above 2000 K, three more bands should become observable.

4.1.3 Resonant Interactions

When two vibrational levels, only one of which can be a fundamental, have the same symmetry and have nearly the same energy, that is, may be accidentally degenerate, they can interact to produce a perturbation called Fermi resonance. The result of such an interaction is that the levels "repel" each other and there is a mixing of intensity. In water this occurs between states having the following quantum number relations: $(n_1 + 2, n_2, n_3)$ and $(n_1, n_2, n_3 + 2)$. Of the states shown in the table only (200) and (210) are effected states. In these cases the perturbations are small and these states do not contribute significantly to the observable spectrum.

4.1.4 Fermi Resonance

In the previous section, the strong resonant interaction between $2\nu_1$ (7201.40 cm^{-1}) and $2\nu_3$ (7445.00 cm^{-1}) was shown not to contribute to the observed spectrum. There is also a weak interaction between ν_1 (3657.054) and $2\nu_2$ (3151.631). For Fermi resonance between two energy levels,

$$\Delta^2 = 4/W_{12}^2 + \delta^2 \quad (4-17)$$

where Δ is the perturbed observed separation, δ is the unperturbed separation, and W_{12} is the energy of interaction and is related to the anharmonic force constant K_{122} by

TABLE 5

VIBRATIONAL TRANSITIONS AND RELATIVE INTENSITIES
AT VARIOUS TEMPERATURES IN THE ν_1 REGION

Transition		Lower State Energy (cm^{-1})	Upper State Energy (cm^{-1})	Band Center (cm^{-1})	Relative Intensity						
Lower State Quantum Numbers	Upper State Quantum Numbers				300 (K)	1000 (K)	1250 (K)	1500 (K)	1750 (K)	2000 (K)	3000 (K)
(000)	(100)	0*	3650.0	3650.0	1.000	1.000	1.000	1.000	1.000	1.000	1.000
(010)	(110)	1590.0	5225.0	3630.0	0.000	0.101	0.160	0.217	0.269	0.317	0.466
(020)	(120)	3151.0	6761.0	3610.0	0.000	0.011	0.027	0.049	0.075	0.104	0.221
(100)	(200)	3650.0	7212.2	3562.2	0.000	0.005	0.015	0.030	0.050	0.072	0.174
(001)	(101)	3755.4	7250.4	3495.0	0.000	0.005	0.013	0.027	0.046	0.067	0.165
(030)	(130)	4668.0	8257.9	3589.9	0.000	0.001	0.005	0.011	0.022	0.032	0.101
(110)	(210)	5225.0	8767.2	3542.2	0.000	0.001	0.002	0.007	0.014	0.023	0.081
(011)	(111)	5330.6	8805.5	3474.9	0.000	0.000	0.002	0.006	0.012	0.022	0.078
(040)	(140)	6146.0	9715.9	3569.9	0.000	0.000	0.001	0.003	0.006	0.012	0.052

* Assigned value

TABLE 6

GROUND VIBRATIONAL STATE
ROTATIONAL ENERGY LEVELS FOR J=0 TO 5

$J(K_{-1}K_1)$	$E \text{ (cm}^{-1}\text{)}$	Relative Population at		
		300 K	1000 K	2000 K
0(0,0)	0	1.00	1.00	1.00
1(0,1)	23.8	0.89	0.97	0.98
1(1,1)	37.1	0.84	0.95	0.97
1(1,0)	42.3	0.82	0.94	0.97
2(0,2)	70.2	0.71	0.90	0.95
2(1,2)	79.5	0.68	0.88	0.94
2(1,1)	95.2	0.63	0.87	0.93
2(2,1)	135.0	0.52	0.82	0.91
2(2,0)	136.0	0.52	0.82	0.91
3(0,3)	136.9	0.52	0.82	0.91
3(1,3)	142.9	0.52	0.82	0.91
3(1,2)	170.6	0.44	0.78	0.90
3(2,2)	206.4	0.37	0.74	0.86
3(2,1)	232.7	0.33	0.72	0.85
3(3,1)	286.6	0.25	0.66	0.81
3(3,0)	286.8	0.25	0.66	0.81
4(0,4)	222.3	0.34	0.73)	0.85
4(1,4)	225.0	0.34	0.73	0.85
4(1,3)	275.9	0.27	0.67	0.82
4(2,3)	300.6	0.24	0.65	0.81
4(2,2)	316.9	0.22	0.63	0.80
4(3,2)	383.8	0.16	0.58	0.76
4(3,1)	385.2	0.16	0.58	0.76
4(4,1)	484.6	0.10	0.50	0.71
4(4,0)	487.7	0.10	0.50	0.71
5(0,5)	325.9	0.21	0.63	0.79
5(1,5)	327.1	0.21	0.63	0.79
5(1,4)	400.4	0.15	0.56	0.75
5(2,4)	416.9	0.14	0.55	0.74
5(2,3)	447.8	0.12	0.53	0.72
5(3,3)	505.6	0.09	0.48	0.69
5(3,2)	510.7	0.09	0.47	0.69
5(4,2)	615.2	0.05	0.41	0.64
5(4,1)	615.5	0.05	0.41	0.64
5(5,1)	758.5	0.03	0.34	0.58
5(5,0)	758.5	0.03	0.34	0.58

TABLE 7THE CONSTANTS α_i FOR THE WATER MOLECULE (cm^{-1})

Vibration	α_i^A	α_i^B	α_i^C
1	+0.495	+0.224	+0.145
2	-2.659	-0.202	+0.105
3	+1.234	+0.112	+0.169

TABLE 8ROTATIONAL CONSTANTS FOR THE GROUND
AND GENERAL EXCITED STATES OF WATER (cm^{-1})

Vibrational State	A	B	C	b
000	27.795	14.508	9.289	-0.1642
100	27.300	14.284	9.144	-0.1649
010	30.454	14.710	9.184	-0.1492
110	29.959	14.486	9.039	-0.1497
020	33.113	14.912	9.079	-0.1381
120	32.618	14.688	8.934	-0.1383

$$W_{12} = (n_1, n_2, n_3 / H^1 / n_1 - 1, n_2 + 2, n_3) =$$

$$\frac{k_{122}}{2} \frac{n_1}{2} (n_2 + 1) (n_2 + 2)^{1/2} \quad (4-18)$$

Since k_{122} has been found to be 71.71 cm^{-1} , then W_{12} for the interaction of v_1 with $2v_2$ is 35.86 cm^{-1} . Then for a $\Delta = 505.423 \text{ cm}^{-1}$, $\delta = 500.310 \text{ cm}^{-1}$. The Fermi shift (F_a) is

$$F_a = (\Delta - \delta) / 2 = 2.557 \text{ cm}^{-1} \quad (4-19)$$

The unperturbed frequency $(v_1)^\circ$ is 3654.497 cm^{-1} .

Since the observed band centers are already known from high resolution infrared work, the Fermi resonance calculation is really incidental to the problem, which is to calculate the observed rotation-vibration band envelope in the v_1 region.

As shown in the previous section, the only hot band significantly contributing to our spectrum is $(v_1 + v_2 - v_2)$ or $(010) \rightarrow (110)$. Now (110) and (010) have been observed at 5235.00 and 1594.59 cm^{-1} respectively. The observed (perturbed) hot band taking the difference is at 3640.41 cm^{-1} . The unperturbed band center of the hot band with $W_{12} = 62.10$ and $\Delta = 568.30 \text{ cm}^{-1}$ is at 3626.67 cm^{-1} . Due to the larger interaction constant, the Fermi shift is 13.74 cm^{-1} in the hot band versus 2.56 cm^{-1} in the fundamental. For our purposes, use of $v_1 = 3657.05$ and $v_1 + v_2 - v_2 = 3640.41$, the observed band centers inherently includes corrections for Fermi resonance. The frequencies presented here vary slightly from those used initially since we are now using a set of frequencies and constants compiled by D. Smith and J. Overend⁽⁵⁾, which we believe are the most up-to-date and accurate of those published.

4.1.5 The Rotational Structure of Vibrational Bands

Our discussion so far pertains to the calculation of the vibrational band centers. About each band center is a rotational manifold representing transitions having the same change in vibrational quantum numbers but different in their rotational quantum numbers.

4.1.5.1 Asymmetric Top Rigid Rotor

Using the geometry shown in Figure 21 and assigning the molecule fixed axis XYZ according to Section 4.1.1, the instantaneous moments of inertia,

$$I_{XX} = \sum_{i=1}^N m_i (y_i^2 + z_i^2), \text{ etc.} \quad (4-20)$$

are $I_{XX} = 1.02024 \times 10^{-40} \text{ g cm}^2$, $I_{YY} = 2.93786 \times 10^{-40}$, and $I_{ZZ} = 1.91762 \times 10^{-40}$. The instantaneous products of inertia

$$I_{XY} = \sum_{i=1}^N m_i x_i y_i, \text{ etc.} \quad (4-21)$$

are $I_{XY} = I_{YZ} = 0$. When the cross terms of the inertial tensor are zero, the diagonal terms are the principal moments of inertia. When all three moments of inertia are different, the molecule is called an asymmetric top. It is customary in molecular spectroscopy to designate these axes as a, b, c with $I_a < I_b < I_c$. It is also convenient to use the rotational constants

$$A = h^2 / 2cI_a, \text{ etc.} \quad (4-22)$$

with $A > B > C$. For water the rotational constants are (all in cm^{-1}):

$$\begin{aligned} A_e &= 27.4355 & A_o &= 27.795 \\ B_e &= 14.5966 & B_o &= 14.508 \\ C_e &= 9.5276 & C_o &= 9.289 \end{aligned} \quad (4-23)$$

The first set of constants in equation (4-23) are for the equilibrium configuration while the second set are for the ground vibrational state. Their difference will be discussed later. The energy matrix for the rotational states with the quantum numbers J and K and using the following notation for matrix elements:

$$(J, K | H_R | J', K') = \int \psi_R^*(J, K) H_R \psi_R(J', K') d\tau \quad (4-24)$$

where for the rigid rotor the Hamiltonian is

$$H_R = 1/2 \left[\frac{P_X^2}{I_X} + \frac{P_Y^2}{I_Y} + \frac{P_Z^2}{I_Z} \right] \quad (4-25)$$

The matrices are

$$(J, K | H_R | J, K) = 1/2 (A_o + C_o) [J(J+1) - K^2] + 2B_o K^2$$

$$\begin{aligned} (J, K | H_R | J, K \pm 2) &= 1/4 (C_o - A_o) \left\{ [J(J+1) - K(K \pm 1)] \right. \\ &\quad \left. [J(J+1) - (K \pm 1)(K \pm 2)] \right\}^{1/2} \end{aligned} \quad (4-26)$$

where $K = -J, \dots, 0, \dots, J$

Equation (4-26) will give a symmetric matrix of the following type for each value of J.

$\begin{array}{c c} & K' \\ \hline K & \end{array}$	-J	-J+1	-J+2	-J+3		J
-J	K_0	0	b_1	0
-J+1	0	K_1	0	b_2
-J+2	b_1	0	K_2	0
-J+3	0	b_2	0	K_3
...
J	K_{J+1}

(4-27)

To simplify calculations this matrix can always be transformed (block diagonalized) into four submatrices labeled E^+ , E^- , 0^+ , 0^- where E^+ means having an element where K is even and positive. Diagonalization of these matrices gives the rotational energy levels. A program was developed to calculate these energy levels for each J.

The Wang asymmetry parameter, (often used to describe vibration-rotation spectra)

$$b = \frac{C-B}{2[A-1/2(B+C)]} \quad (4-28)$$

is a measure of a molecule's asymmetry. For the equilibrium constants in equation (4-23), $b = 0.1649$. In the prolate limit, $A > B = C$, $b = 0$ and in the oblate limit, $A = B > C$, $b = -1$. Typical asymmetric energy levels for low J are shown in Figure 23. Note that it is best to show water as a perturbation

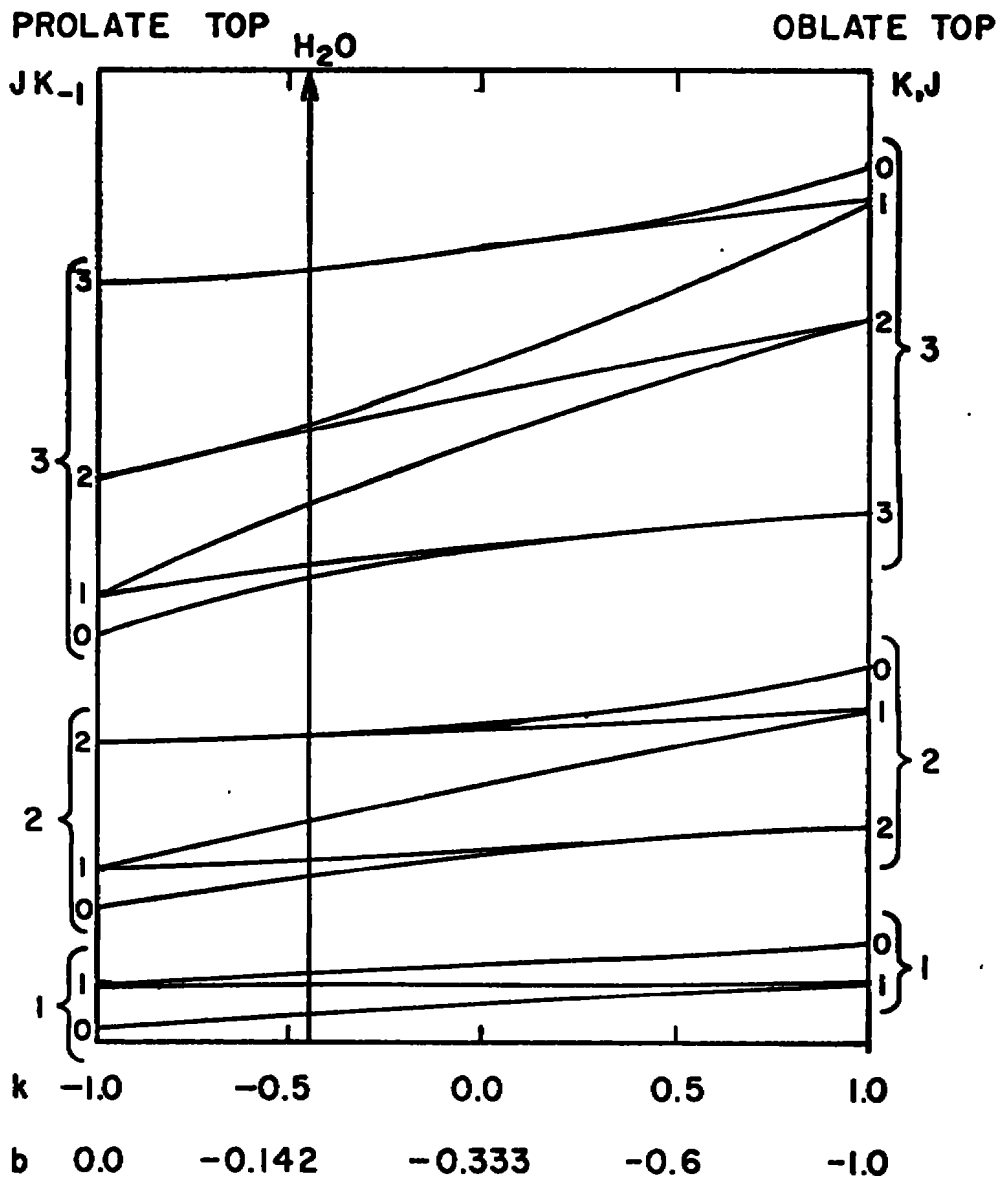


FIGURE 23
ASYMMETRIC ENERGY LEVELS FOR LOW J

of the prolate limit rather than of the oblate limit. Another way to designate the energy levels is the bipartite index $K_{-1}K_1$ where these are the energy levels in the prolate and oblate limits respectively. Also

$$K = K_{-1} - K_1 \quad (4-29)$$

The energy levels for $J = 0$ to 5 are shown in Table 6 along with the relative population at various temperatures. Unlike those intensity values in Table 5, the transition probabilities for rotation are not constant over J and K_{-1} . Therefore, the relative population of the levels is not a measure of the relative intensity. The rotational line strengths will be considered later; however, they increase more rapidly with K_{-1} than with J . The low K_{-1} levels of high J contribute extensively to the observed band shape.

4.2 CALCULATION OF THE ROTATION-VIBRATION SPECTRA IN THE ν_1 REGION OF WATER VAPOR

4.2.1 Higher Order Approximation to the Energies of an Asymmetric Rotor - Artificial Distortion

The effects due to centrifugal distortion are usually too small to observe at frequency accuracy and resolutions of less than 0.1 cm^{-1} . The treatment of the non-rigid rotor adds terms of the following type to the energy matrix: (K/K) , $(K/K \pm 2)$, and $(K/K \pm 4)$. A better (should converge more rapidly) equation for the diagonal elements than the one shown previously includes the centrifugal stretching constants:

$$E = \frac{B+C}{2} J(J+1) + \left(A - \frac{B+C}{2} \right) K^2 \quad (4-30)$$

$$- D_J J^2 (J+1)^2 - D_{JK} J(J+1) K^2 - D_K K^4$$

The last terms in equation (4-30) are due to centrifugal distortion. It is easily observed that these terms become significant at high J and K . The exact values for D_J , D_{JK} and D_K have not as yet been determined, but they are on the order 10^{-4} to 10^{-5} cm^{-1} . But as we have shown, the selection rules are $\Delta J = 0$ and $\Delta K = 0$. Hence, the shift in spectral lines should have the form:

$$(D_{v_1} - D_0) J^2 (J+1)^2 + J(J+1) K^2 + K^4 \quad (4-31)$$

where $D_{v_1} - D_0$, the change in centrifugal distortion between the ground state and v_1 , is at most of the order 10^{-6} cm^{-1} . For example, a line that should contribute to our observed spectrum is $J = 20$ and $K = 9$, is shifted only 0.2 cm^{-1} .

4.2.2 Higher Approximations to the Energies of an Asymmetric Rotor

4.2.2.1 Rotation-Vibration Interaction

The rotational constants of excited vibrational states will be different from those in the ground state since the geometry of the molecule changes with excitation. This dependency has been determined, using harmonic oscillator wave functions, and is as follows:

$$A_v = A_e - \sum \alpha_i^A (n_i + 1/2), \text{ etc.} \quad (4-32)$$

Since this is a small perturbation to the rigid rotor energy levels, the harmonic approximation is adequate. For water the constants α_i are shown in Table 7. The rotational constants for the vibrational states involved in the fundamental and the two most intense hot bands as calculated in Table 5 are tabulated in Table 8. The tabulation of the Wang asymmetry parameter shows there is very little change in asymmetry for $\Delta n_1 = 1$, and hence this does not contribute to the band structure.

4.3 CORIOLIS PERTURBATION

Two vibrations may interact through Coriolis coupling when the "product" of their species contains the species of a rotation of the molecule (Jahn's rule). The interaction is significant only when the two vibrations are nearly degenerate. For water ν_1 at 3652 cm^{-1} and ν_3 at 3756 cm^{-1} are close enough to strongly interact and

$$A_1(\nu_1) \times B_1(\nu_3) = B_1(R_Y). \quad (4-33)$$

Since Y has been identified with the rotation constant C, this will be C-type Coriolis Coupling whose nonvanishing matrix elements are

$$(\nu_1, J, K | H_1' | \nu_3, J, K \pm 1) = i f(J, K, \pm) R_1^C \quad (4-34)$$

and

$$(\nu_3, J, K | H_1' | \nu_1, J, K \pm 1) = -i f(J, K, \pm) R_1^C \quad (4-35)$$

where

$$R_1^C = \zeta_{13}^Y C_e \left[\frac{\omega_1 + \omega_3}{(\omega_1 \omega_3)^{1/2}} \right]$$

$$i = \sqrt{-1}$$

and

$$f(J, K, \pm) = \frac{1}{2} [J(J+1) - K(K \pm 1)]^{1/2}$$

TABLE 9
CALCULATED AND OBSERVED Q BRANCH TRANSITIONS BETWEEN
THE VIBRATIONAL STATES (000) AND (100) FOR H₂O VAPOR

State	Observed (cm ⁻¹)	Calculated (cm ⁻¹)
$J(k_{-1}, k_1)$		
0(0, 0)	3657.054	3657.054
1(0, 1)	3656.66	3656.695
1(1, 1)	3656.171	3656.414
1(1, 0)	3656.114	3656.335
2(0, 2)	3655.85	3655.962
2(1, 2)	3655.41	3655.755
2(1, 1)	3655.29	3655.518
2(2, 1)	3653.79	3654.691
2(2, 0)	3653.81	3654.705
3(0, 3)	3654.62	3654.907
3(1, 3)	3654.26	3654.774
3(1, 2)	3655.03	3654.302
3(2, 2)	3652.58	3653.598
3(2, 1)	3652.62	3653.531
3(3, 1)	3649.98	3652.037
3(3, 0)	3649.93	3652.036
4(0, 4)	3652.95	3653.553
4(1, 4)	3652.73	3653.480
4(1, 3)	3652.28	3652.699
4(2, 3)	3650.96	3652.133

TABLE 9. (Continued)

4(2, 2)	3650.77	3651.943
4(3, 2)	3648.34	3650.537
4(3, 1)	3648.02	3650.529
4(4, 1)	3646.86	3648.385
4(4, 0)	3646.64	3648.385
5(0, 5)	3650.95	3651.916
5(1, 5)	3650.83	3652.880
5(1, 4)	3650.08	3650.731
5(2, 4)	3648.94	3650.318
5(2, 3)	3649.41	3649.921
5(3, 3)	3646.36	3648.658
5(3, 2)	3645.12	3648.621
5(4, 2)	3647.65	3646.509
5(4, 1)	3645.89	3646.509
5(5, 1)	3640.00	3643.743
5(5, 0)	3639.81	3643.743

ζ_{13}^Y is the Coriolis coupling constant. For each J , there will be a Hermetian matrix ($a_{ij} = a_{ji}^*$ where $*$ means complex conjugate) of order $4J + 2$. If v_i are the $2J + 1$ matrices described in Section 4.1.5.1, the block diagonalized energy matrix will have the form

$$\begin{vmatrix} v_1 & \omega_{12} \\ \omega_{12}^* & v_3 \end{vmatrix} \quad (4-36)$$

where ω_{12} is $2J + 1$ matrix with the elements described in equation (4-34). This matrix can be further block diagonalized into four submatrices of $J + 1$, $J + 1$, J and J dimensions where the interacting sets of rotation-vibration states will be: $E^- \longleftrightarrow 0^+$ and $E^+ \longleftrightarrow 0^-$.

Fraley and Rao⁽⁶⁾ give the observed energy levels of H_2O up to $J = 9$ for the vibrational states (000), (100), and (001). We have calculated the ground state levels for up to $J = 5$ without including the effects of Coriolis interactions. The comparison of the observed and calculated results, Table 9, shows maximum differences of no greater than 1 to 2 cm^{-1} . Thus, we can assume that Coriolis coupling can be neglected for low values of J . For large values of J , $J > 15$, this interaction may yet have to be included in the calculations. This will be determined when the initial calculations are carried out for temperatures greater than 1000 K.

4.4 SELECTION RULES FOR A-TYPE BANDS IN AN ASYMMETRIC TOP

Once the energy levels of the upper and lower states have been determined, the selection rules tell us what transitions can occur. The selection rules for Raman transitions where only α_{XX} , α_{YY} , and α_{ZZ} are different from zero are:

$$\Delta J = 0, \pm 1, \pm 2$$

ee ee

eo eo

oe oe

oo oo

(4-37)

where ee etc, refer to the bipartite notation $K_{-1}K_1$ and means both K_{-1} and K_1 are even. The dominant transitions are those where $\Delta J = 0$, the so called Q branch. This sharp strong central "line" will in general be the only feature that is observed. The changes ΔK_{-1} and ΔK_1 can be 0, ± 2 , ± 4 , . . . However, those with ΔK_{-1} and $\Delta K_1 = 0$ will be dominant. Consequently the rotational structure about ν_1 and its hot bands will be primarily transitions where

$$n_1, J(K_{-1}, K_1) \rightarrow n_1 + 1, J(K_{-1}, K_1). \quad (4-38)$$

There are two reasons why these lines do not exactly coincide:

- (a) the asymmetry of the molecule changes on excitation of ν_1 . This was shown in Table 8 to be relatively small.
- (b) Coriolis coupling with ν_3 .

4.5 CALCULATION OF RELATIVE LINE STRENGTHS

The transition probability for Raman lines is

$$| (V, R | \bar{P}^0 | V', R') |^2 \quad (4-39)$$

where $\bar{P}^\circ = \alpha \bar{E}$. P° , the time-independent induced dipole moment is equal to the polarizability, α , times the applied field.

$$\left| \sum_g E_g^\circ \sum_{g'} (V, R | \alpha_{gg'} | V', R') \right|^2 \quad (4-40)$$

It is possible to separate the rotation and vibration parts of the integral in equation (4-40) as follows

$$(V, R | \alpha_{gg'} | V', R') = (V | \alpha_{gg'} | V') (R | \Phi_{Fg} \Phi_{Fg'} | R') \quad (4-41)$$

It is not necessary to know the exact values of the $(V | \alpha_{gg'} | V')$, merely that the quantity is nonvanishing. Hence the line strengths can be defined as

$$\sum_{Fg} | (R | \Phi_{Fg} \Phi_{F'g'} | R'') |^2 \quad (4-42)$$

and, by combining these appropriately with the lower state Boltzmann population, the relative intensities of vibrational rotational transitions may be calculated. The Coriolis coupling leads to an intensity perturbation also and must be taken into account. The eigenvectors determined in the diagonalization of the $4J + 2$ Hermitian matrix can be used to find the degree of v_3 character in the line. Since in the Raman spectrum the intensity of v_3 is nearly zero, multiplication by one minus this factor will be used to reduce the intensity.

4.6 CALCULATION OF THE BAND ENVELOPE

Once the intensity and frequency of the component lines have been determined, the overall band envelope at a given temperature can be determined.

Gaufres⁽⁷⁾ gives for the intensity of a vibration-rotation Raman line

$$I_{\rho\sigma}(V', J', n', M' \rightarrow V'', J'', n'', M'') \propto \sum_{j, k} |\langle V'' | \alpha_{jk} | V' \rangle|^2 |\langle J'', n'', M'' | \phi_{\rho\sigma jk} | J', n', M' \rangle|^2 \quad (4-43)$$

A vibrational band is allowed when at least one of the six different elements of $\langle V'' | \alpha_{jk} | V' \rangle$ is non-vanishing, while the rotational structure of an allowed band arises from the non-vanishing elements of the second term of the product. In expression 4-43, the molecular coordinates are represented by ρ and σ , the laboratory coordinates by j and k , the single prime and double prime denotes the upper and lower states of the vibrational, rotation and magnetic quantum states respectively for V , J , M and n where n represents a rotational quantum number other than J . The term α_{jk} is the polarizability tensor of the molecule and $\phi_{\rho\sigma jk}$ is the orientation matrix of the molecule in the laboratory reference frame. Its elements are the Euler angles defined by the system.

The polarizability tensor may be written as

$$\begin{vmatrix} \alpha_{xx} & \alpha_{xy} & \alpha_{xz} \\ \alpha_{yx} & \alpha_{yy} & \alpha_{yz} \\ \alpha_{zx} & \alpha_{zy} & \alpha_{zz} \end{vmatrix} = \begin{vmatrix} \alpha & 0 & 0 \\ 0 & \alpha & 0 \\ 0 & 0 & \alpha \end{vmatrix} + \begin{vmatrix} \alpha'_{xx} & \alpha'_{xy} & \alpha'_{xz} \\ \alpha'_{yx} & \alpha'_{yy} & \alpha'_{yz} \\ \alpha'_{zx} & \alpha'_{zy} & \alpha'_{zz} \end{vmatrix} \quad (4-44)$$

in which

$$\alpha = \frac{1}{3} (\alpha_{xx} + \alpha_{yy} + \alpha_{zz})$$

and

$$\alpha'_{jj} = \alpha_{jj} - \alpha$$

and

$$\alpha'_{jk} = \alpha_{jk} \quad (j \neq k).$$

The trace of the LHS of equation 4-44 is given by the first term of the RHS of equation 4-44 and the anisotropy of α_{ij} is given by the second term in the RHS. The selection rules for trace scattering are known to be: ⁽⁷⁾

$$J' = J'', n' = n'', \text{ and } M' = M''.$$

Thus, trace scattering can only be in the Q branch ($\Delta J = 0$), whereas the anisotropy scattering occurs from O, P, R, and S branches ($\Delta J = \pm 1, \pm 2$).

The trace scattering and the anisotropy scattering may be separated experimentally since the polarized spectra, $I_{||}$, and the dipolarized spectra, I_{\perp} , are functions of the trace and anisotropy scattering:

$$I_{||} \propto 45I_{tr} + 4I_{anis} \quad (4-45)$$

$$I_{\perp} \propto 3I_{anis}$$

We have shown experimentally that the water vapor spectrum may be safely approximated as only trace scattering.

Gaufres gives for the line intensity of trace scattering for asymmetric tops the following expression:

$$I(J) = F(J) \times (2J + 1)g'' \exp(-E''_{rot}/kT) \quad (4-46)$$

In this expression the pre-exponential term $F(J)$ is approximated to be unity. This is only valid for isotropic scattering; for anisotropic scattering $F(J)$ becomes a complicated function dependent on symmetry. The term E''_{rot} is the ground state energy level of the transition. The theoretical evaluation of it has been discussed previously. The term g'' is the nuclear spin degeneracy in the initial state. For the water molecule it has a value of 3 for symmetric states and 1 for anti-symmetric states. ⁽⁸⁾

SECTION V

CALCULATED RAMAN BAND PROFILES OF THE ν_1 REGION OF H_2O VAPOR5.1 COMPUTER PROGRAM FOR CALCULATION OF THE Q BRANCH OF H_2O VAPOR IN THE ν_1 REGION

The problem of calculating the Raman band profile of water vapor in the ν_1 region is greatly simplified by the absence of any significant contributions from anisotropic scattering. This fact was clearly demonstrated in Section 3.3 in the discussion of the polarized Raman spectra. The selection rules for the water molecule predict that only the Q-branch of the rotation-vibration transition manifold may be active in isotropic Raman scattering.

5.1.1 Limitations and Description of Calculations

A computer program was generated (Appendix) to calculate the Raman band profile of H_2O vapor. The program was written in such a manner as to design a theoretical model which reproduced the experimental observation as closely as possible. For example, the experimental spectra were obtained with a spectral slit width of 8 cm^{-1} ($\approx 3\text{ \AA}$) and the computer program uses a slit function with the same width. No provisions were made for changing this function with external input statements.

Since the calculation involves analyzing very low resolution spectra, the perturbation of line position due to centrifugal distortion and Coriolis coupling, and the effects of pressure broadening doppler shifts and natural line widths were not included in the calculation of the contour shapes. These effects, which perturb the line widths of the Q branch of H_2O by tenths of wavenumbers and the line positions by less than a wavenumber, are insignificant in the 8 cm^{-1} spectrally resolved spectra.

The computer program which was written is thus severely limited in application. It can only reproduce the first three vibrational hot bands of the ν_1 band of H_2O and their Q branches. It may only calculate with any degree of certainty low resolution spectra (8 cm^{-1}). The program includes no provisions for higher perturbations to the line positions or line intensities.

The program used the Scientific Subroutine "EIGEN" for diagonalizing the energy matrices. The program calculates the eigen values for J maximum of 30.

5.1.2 Slit Function

To reproduce theoretically an experimentally obtained band shape, it is necessary to use a theoretical instrument function that closely resembles the actual instrument function. In practice, workers have successfully used both Gaussian and triangular slit functions. In order to determine which function best fits our instrument function, the instrument slit function was determined experimentally. It was observed, Figure 24, that a triangular function more closely resembled the low resolution instrument function than did the Gaussian function. This instrument function was determined by scanning a laser line of width $\approx 0.1\text{ cm}^{-1}$ with the monochromator set at 8 cm^{-1} . Therefore, the triangular slit function was used in these present calculations.

5.1.3 Computer

The computer program was written in Fortran IV language for use on a Data General - NOVA computer. Since the core size of this computer is small, it was necessary to break up the large program into four smaller ones. The NOVA computer with disk

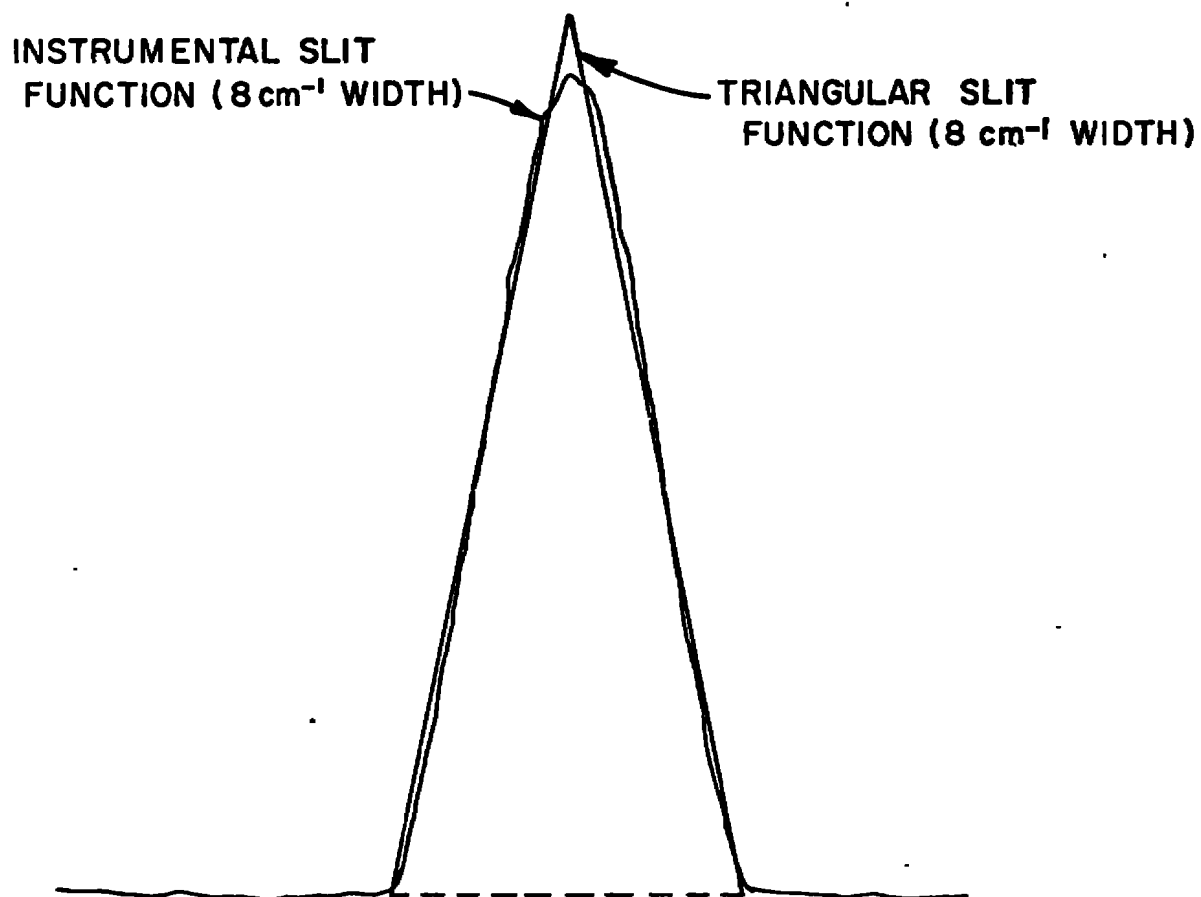


FIGURE 24
COMPARISON OF INSTRUMENT AND THEORETICAL SLIT FUNCTIONS

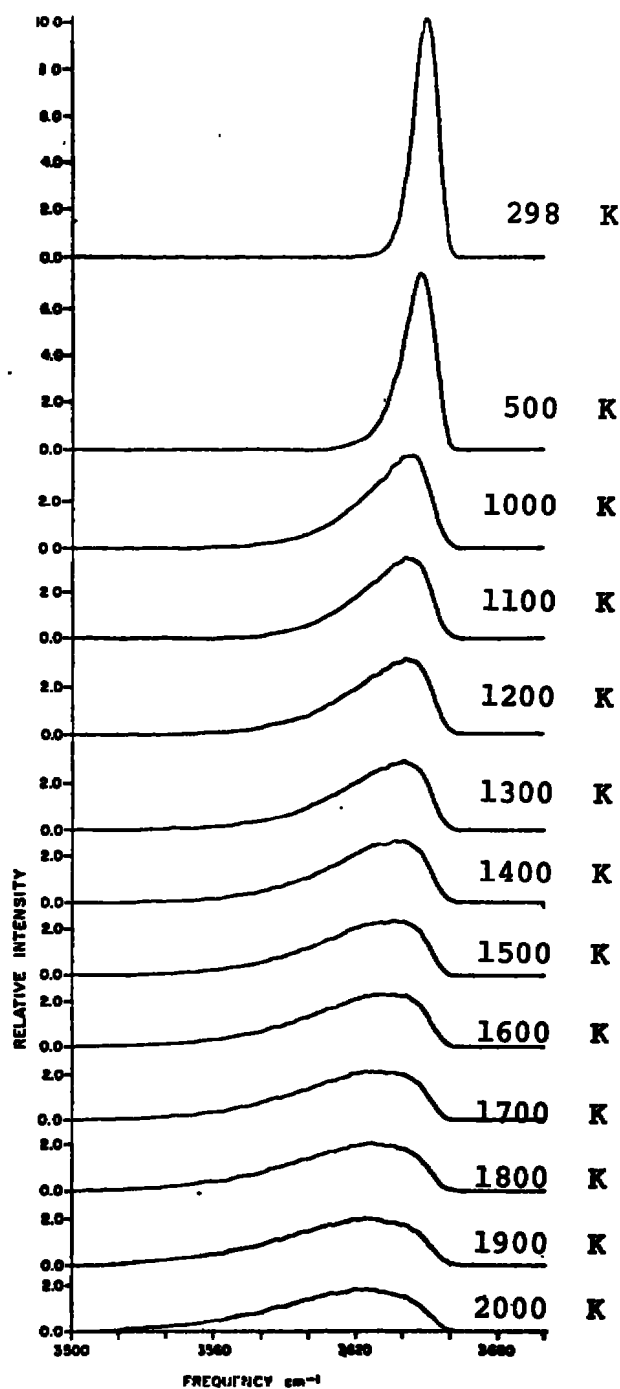


FIGURE 25
CALCULATED RAMAN BAND PROFILES OF H₂O
IN THE ν_1 REGION OF H₂O VAPOR (8 CM⁻¹ RESOLUTION)
AT VARIOUS TEMPERATURES RELATIVE TO 298 K.

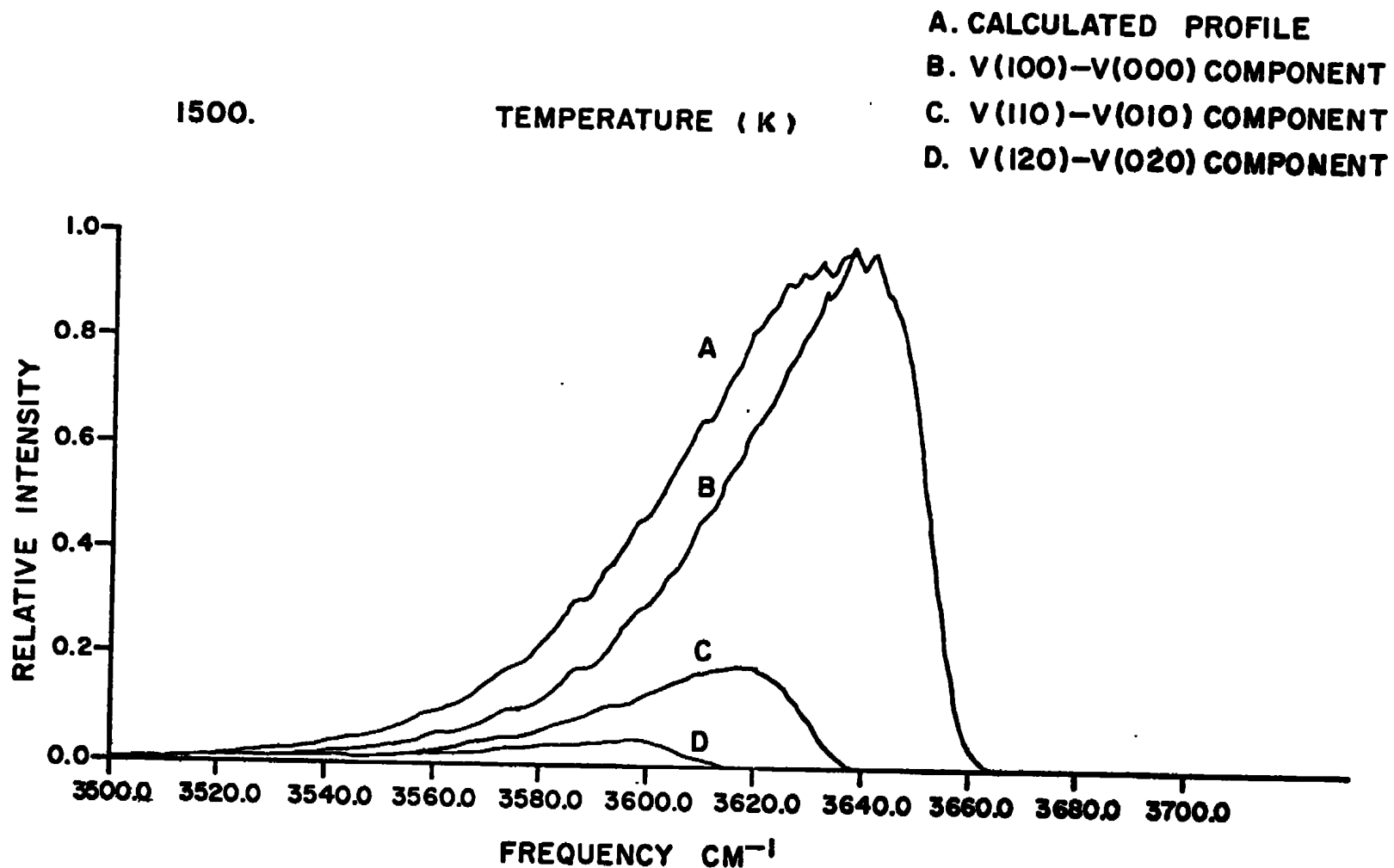


FIGURE 26
THE VIBRATIONAL HOT BAND COMPONENTS OF H_2O

5.4 THEORETICAL LINE ANALYSIS

The calculated Raman band contours of water vapor at 1500 K are shown in Figures 27 to 29 for the (100)+(000) transition with slit functions of 8, 4 and 2 cm^{-1} respectively. The low resolution contour lacks fine structure, however at increasingly higher resolution a definite fine structure which is only slightly regular appears.

The pattern which is quite clear in the 2 cm^{-1} slit function contour is unexpected and not predicted as a highly asymmetric top such as H_2O should not have a regular pattern in its Q branch.

To determine the reason for the peculiar fine structure in the 2 cm^{-1} contour of Figure 29, it is necessary to analyze which lines and therefore which J and $K_{-1}K_1$ components are contributing to the fine structure. In Table 10 are the component lines which are found to be contributing to the intensity of peaks located at 3631 and 3627 cm^{-1} of Figure 29. Note that the pattern is irregular and that the grouping of the lines to form the fine structure in the calculated contours is merely coincidental.

The overall intensity of the band contour arises from a Boltzmann distribution within the Q branch. In general, it is seen that those lines with low J and K contribute most to the band intensity. The fall-off in intensity as J or K increases is strictly a statistical result. Furthermore, the shift of the line from the band center increases with J and K. At temperatures above 1500 K band contour extends several hundred wave numbers below the band center. An analysis of the line positions and intensities indicated that very little intensity was contributed to the overall band intensity for J values greater than 20 and $J_{\text{MAX}} = 25$ was more than sufficient for calculating the band contour at 2000 K.

RAMAN SPECTRUM OF H₂O

1500.

TEMPERATURE (K)

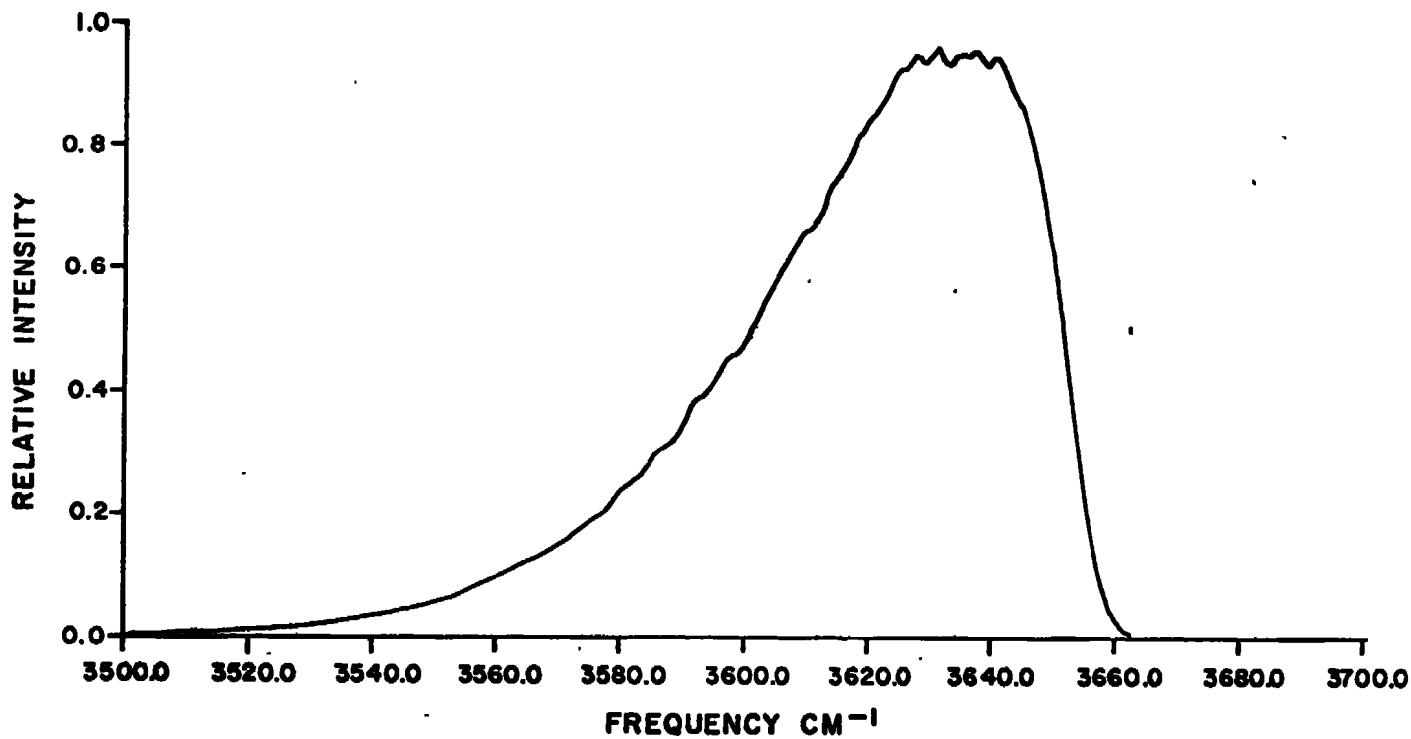


FIGURE 27

CALCULATED H₂O RAMAN SPECTRUM
WITH 8 CM⁻¹ RESOLUTION

RAMAN SPECTRUM OF H₂O

1500.

TEMPERATURE (K)

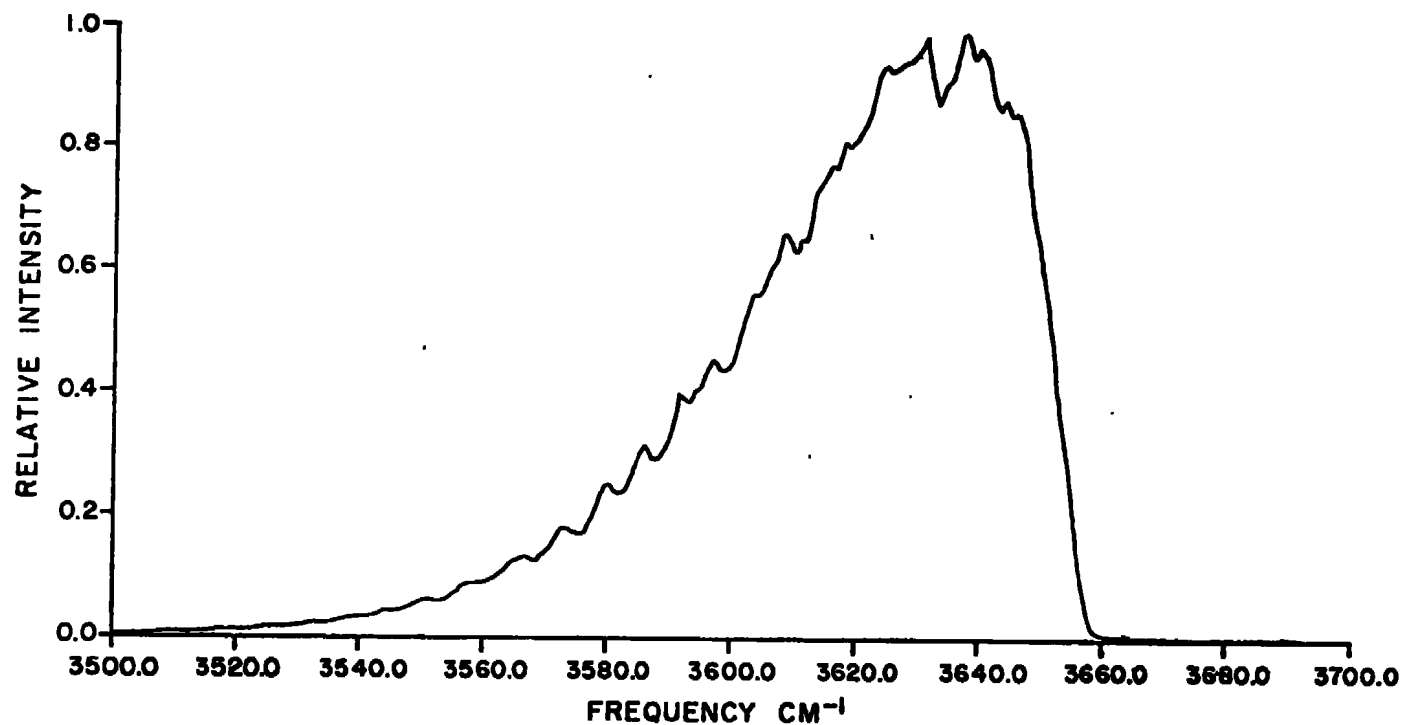


FIGURE 28

CALCULATED RAMAN PROFILE OF H₂O
WITH 4 CM⁻¹ RESOLUTION

RAMAN SPECTRUM OF H₂O

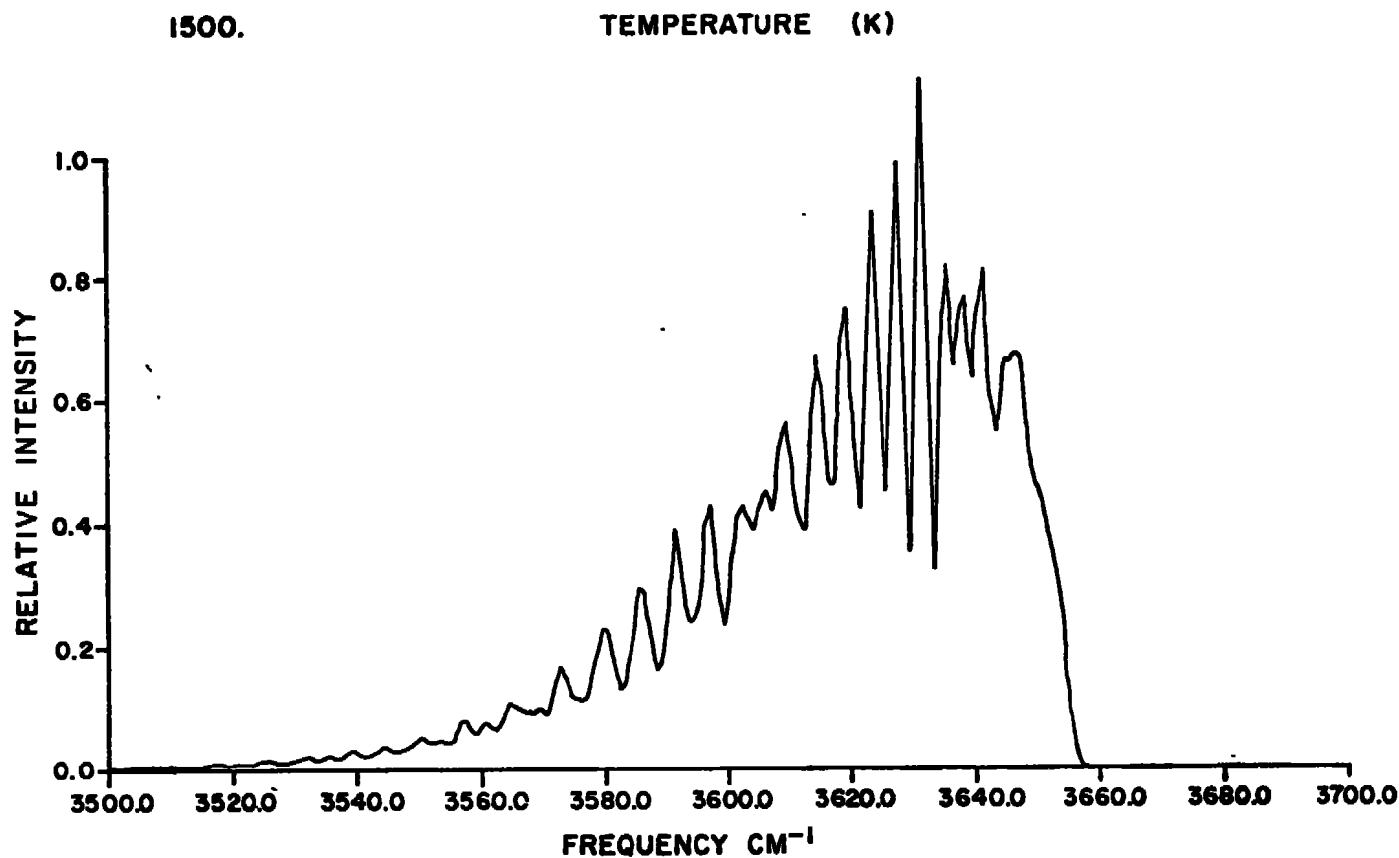


FIGURE 29
CALCULATED RAMAN BAND PROFILE
OF H₂O WITH 2 CM⁻¹ RESOLUTION

TABLE 10
PARTIAL LIST OF LINE POSITIONS

Lines in Region (3629.5→3632.5 cm^{-1})				Lines in Region (3627.5→3629.5 cm^{-1})			
J	K_{-1}	K_1		J	K_{-1}	K_1	
7	(0,7)	(7,0)		8	(1,8)	(5,4)	
8	(1,7)	(5,3)		9	(2,8)	(6,3)	
9	(2,7)	(7,3)		10	(3,8)	(8,3)	
10	(3,7)	(8,2)	(9,2)	11	(4,8)	(9,2)	
11	(4,7)	(10,2)		12	(5,7)	(12,1)	
12	(6,6)	(12,0)		13	(6,7)	(13,0)	

1. The lines in the 3629.5→3632.5 cm^{-1} region correspond to a peak in the 2 cm^{-1} resolution spectra - Figure 29.
2. These lines in the 3627.5→3629.5 cm^{-1} region correspond to a valley in between peaks in Figure 29.

5.5 COMPARISON OF CALCULATED CONTOURS TO OBSERVED CONTOURS

The comparison between the observed Raman band contour and the calculated contours is demonstrated in Figure 30. The observed Raman band profile, obtained at ≈ 1100 K, is plotted with the calculated contours of 1000, 1100 and 1200 K. There appears to be excellent agreement between the calculated temperature profile at 1100 K and the temperature obtained from the H_2O Raman spectrum. These results clearly show that if the signal to noise statistical error is sufficiently low the flame temperatures obtained from an analysis of the Raman band of H_2O are comparable to those previously obtained from analysis of the N_2 band.

The experimental spectra discussed in Section III have an uneven band contour which appears to increase with temperature and at first examination appears to be fine structure. However, the spectra obtained at 1650 and 1750 K do not have this shape in their contours. It is suspected that this structure on the contour arises from Na emission: the spectra obtained between 1000 and 1500 K were carried out by photon counting techniques, whereas the higher temperature spectra were obtained using phase sensitivity detection which eliminated the flame emission problem.

The experimental Raman band profiles show quite clearly the relationship between the asymmetry and the temperature of the water band. A relationship, therefore, should exist between the full width at half height (FWHH) of the Raman band profile and the rotational-vibrational temperature of the water molecules. In Figure 31 a theoretical FWHH versus temperature plot is shown. The experimentally observed FWHH's of the water band at the temperatures determined from the N_2 band analysis have been put

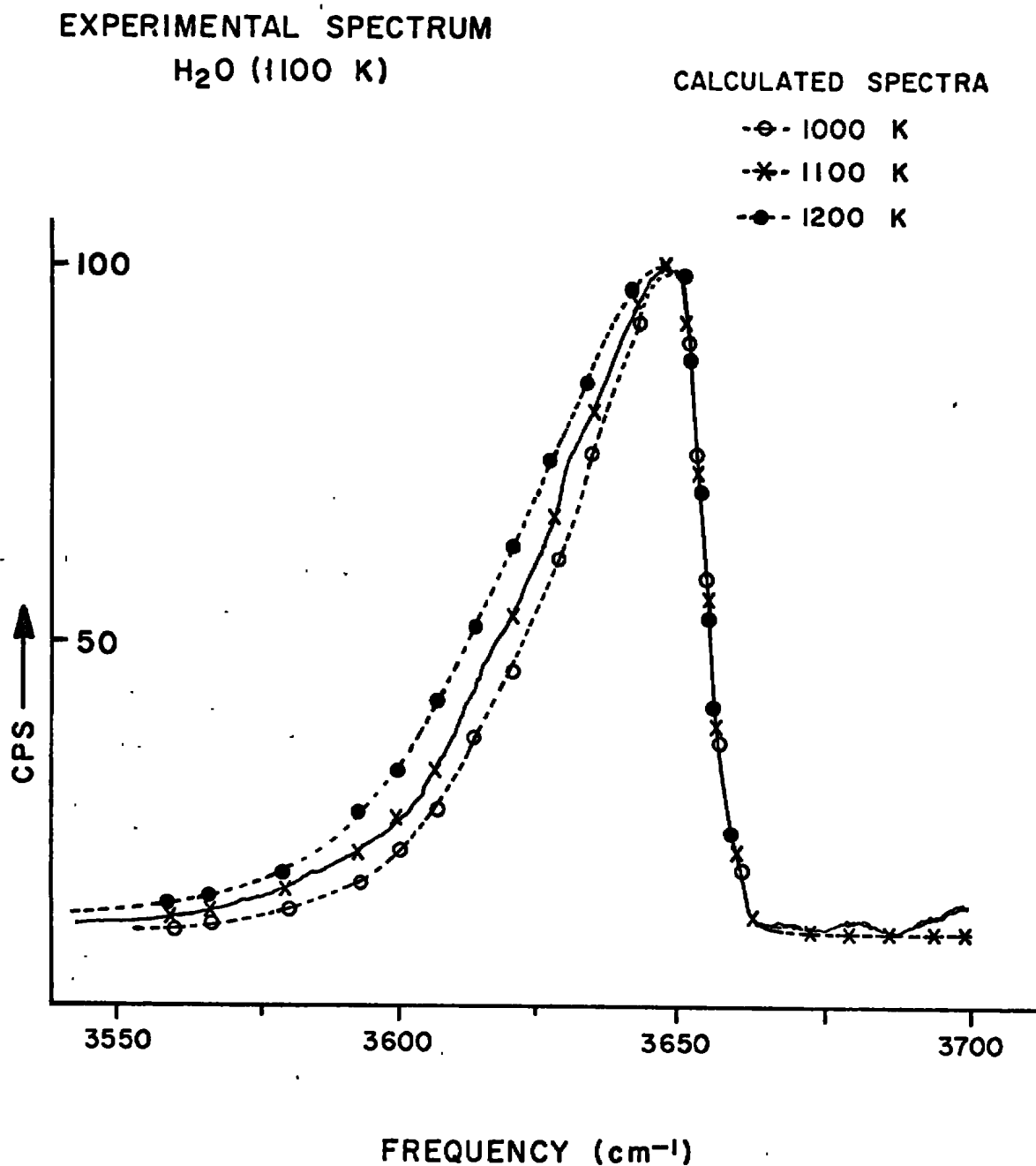


FIGURE 30
COMPARISON OF EXPERIMENTAL
AND CALCULATED RAMAN BAND PROFILES

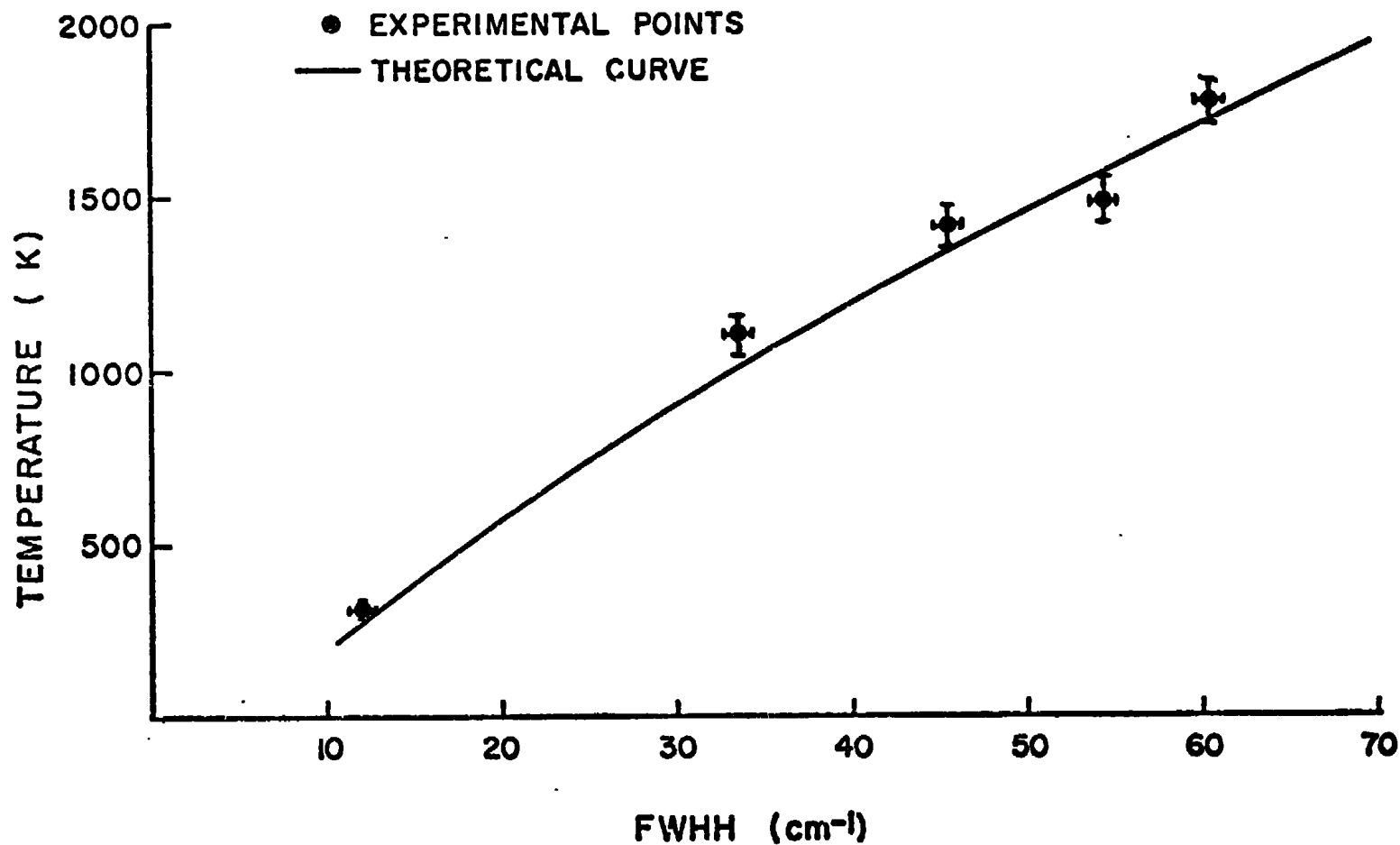


FIGURE 31

PLOT OF TEMPERATURE VERSUS THE FULL WIDTH AT HALF HEIGHT
OF THE EXPERIMENTAL AND THEORETICAL RAMAN BAND CONTOURS OF H₂O VAPOR

in the figure to show the comparison. The error bars shown on this data represent the one sigma error uncertainty in determining the FWHH (± 25 K). Note that within experimental error, the use of the experimentally obtained FWHH's is accurate enough for equilibrium temperature determination of the water molecules in the flame gases.

SECTION VI

CONCLUSIONS AND RECOMMENDATIONS

6.0 SUMMARY OF WORK ACCOMPLISHED

In accordance with the Work Statement for this contract, the work accomplished and submitted in this technical report includes, but is not limited to, the following:

a. Experimental Study

- (i) Results have included Raman Stokes cross sections of H_2O relative to N_2 at room temperature and at a minimum of five temperatures between 1000 - 1750 K. Section III.
- (ii) Verification that temperatures were calibrated using Raman scattering of nitrogen. Section III.
- (iii) Estimates of inhomogeneity of the source temperature and the flame specie number density values are discussed in Section III. Due to the large number of variables present in the experiments, a measurement of these errors was too difficult to obtain.
- (iv) Verification of the wavelength calibration of the monochromator and that the wavelength uncertainty is inconsequential to the spectra obtained. Section III. The instrument was calibrated with lamp standards to an accuracy of $\pm 1 \text{ cm}^{-1}$ and since the present data was low resolution ($\sim 8 \text{ cm}^{-1}$) the wavelength uncertainty can be disregarded.
- (v) The major contributions to the experimental error. Section III.
- (vi) Documentation that studies were performed at a second wavelength to verify that Raman cross-section

scaling varies as the source wavelength to the fourth power. Section III.

b. Theoretical Study

- (i) A computer program (in Fortran IV code) is provided that allows for only the theoretical calculation of the water vapor band Q branch profile at various temperatures. Appendix.
- (ii) Calculated Raman band contours of water vapor in the ν_1 region over a wide range of temperatures. Section V.
- (iii) Experimental verification that the contribution of the anisotropic Raman scattering by the ν_1 band of water vapor is negligible and need not be considered. Section III. This is true only for these low resolution studies. Polarization experiments at high resolution are required for further verification.
- (iv) The results of the theoretical study include an interpretation and correlation of the water vapor spectrum, an analysis of the observed Raman band energy levels in the ν_1 region of water vapor, and a comparison of the observed experimental Raman band contours and the calculated contours.

6.1 USE OF H₂O RAMAN BAND PROFILES FOR TEMPERATURE AND SPECIE DENSITY STUDIES

The results of this study show quite clearly that Raman scattering studies of water vapor can give temperature and specie densities. The work has demonstrated that, if signal-to-noise statistics allow, the Raman data obtained from water vapor gives comparable results to that obtained from N₂ Raman data. The accuracy of these determinations is not greater than ± 50 K for

temperature and not greater than $\pm 10\%$ in number density.

6.2 RECOMMENDATIONS FOR EXTENDED WORK

6.2.1 Modification of the Computer Program

Since this work clearly demonstrates the high degree of success in reproducing theoretically the observed Raman band contours of low resolution H_2O spectra, it is recommended that future work be carried out to extend this study. The study should include the following:

- (1) the generalization of the computer program for calculation of Raman spectra for any molecule of any symmetry in the vapor phase;
- (2) a theoretical study to determine the intensity expressions for the anisotropic Raman scattering of asymmetric tops;
- (3) modification of the program for calculation of theoretical high resolution spectra. This will include the ability to include the effects of Doppler broadening, pressure broadening, centrifugal distortion, Fermi resonance, Coriolis coupling effects, and several kinds of slit functions in the theoretically calculated spectra.

6.2.2 Experimental Work on Other Molecules

It is recommended that Raman scattering experimental studies be carried out on other flame species of interest simultaneously with the theoretical studies proposed. These studies should be carried out to obtain cross sections of interest and to verify the theoretical calculations. The possibility of using Raman scattering spectroscopy in burnt fuel diagnostics has been clearly demonstrated by a number of workers and by this study. Advantage should be taken of this technique and it should be pursued to its fullest.

REFERENCES

- (1) W.E. Kaskan, "6th Symposium (International) on Combustion", Williams and Wilkins Co., Baltimore (1957) p. 134.
- (2) P.J. Padley and T.M. Sugden, Proc. Roy. Soc. A, 248, 238 (1958).
- (3) M. Lapp, Advances in Raman Spectroscopy, Volume 1, edited by J.P. Mathieu, Heyden and Sons (1973) p. 256.
- (4) M. Lapp, L.M. Goldman and C.M. Penney, Science, 175, 1112, (1972).
- (5) D. Smith and J. Overend, Spectrochim. Acta 28A, 471 (1972).
- (6) P.E. Fraley and R.N. Rao, J. Mol. Spectrosc. 29, 348 (1969).
- (7) R. Gaufres, Laser Raman Gas Diagnostics, edited by M. Lapp and C.M. Penney, Plenum Press, New York (1974) p. 15.
- (8) G. Herzberg, Infrared and Raman Spectra, Nostrand, Princeton, N.J. (1945).

APPENDIX

COMPUTER PROGRAM FOR CALCULATING
LOW RESOLUTION RAMAN BAND
PROFILES OF H₂O IN THE
 ν_1 REGION

THIS BRUTE FORCE PROGRAM CALCULATES THE
 TFACE SCATTERING RAMAN BAND PROFILE SPECTRUM
 FOR H2O AT VARIOUS TEMPERATURES UP TO 2000K

C
 DIMENSION A(1326),A1(61),A0(2),B0(2),C0(2),AC(800)

THE FOLLOWING SERIES OF DO LOOPS COMPUTES THE ELEMENTS
 OF THE ENERGY MATRICES FOR THE VIBRATIONAL STATES OF H2O
 (000),(100),(010),(110),(020),(120) FOR VALUES
 OF J UP TO 30

CALL RESET
 CALL FOPEN (0,'A000',4)
 CALL FOPEN (1,'A100',4)
 CALL FOPEN (2,'A010',4)
 CALL FOPEN (3,'A110',4)
 CALL FOPEN (4,'A020',4)
 CALL FOPEN (5,'A120',4)
 III=0
 DO 10 M=1,6
 A0(1)=27.795
 B0(1)=14.508
 C0(1)=9.289
 A0(2)=27.300
 B0(2)=14.284
 C0(2)=9.144
 A0(3)=30.454
 B0(3)=14.170
 C0(3)=9.184
 A0(4)=29.959
 B0(4)=14.486
 C0(4)=9.039
 A0(5)=33.113
 B0(5)=14.912
 C0(5)=9.079
 A0(6)=32.618
 B0(6)=14.688
 C0(6)=8.934
 L=25
 LL=2
 DO 1 J=1,L
 ME=(((2*J)+1)**2+((2*J)+1))/2
 DO 2 JJ=1,ME
 A(JJ)=0.0
 CONTINUE

2


```

      NN=NN+1
12    CONTINUE
      NN=NN+J
11    CONTINUE
      N=J+1
      DO 14 I=1,NU
14    A(I)=AC(I)
      CALL EIGEN (A,R,N,1)
      MM=1
      JJ=2
      N=(2*N)+1
      DO 13 I=NU,N
      A1(I)=A(MM)
      MM=MM+JJ
13    JJ=JJ+1
      CALL FSEEK (III,LL)
      DO 6 I=1,N
      A2=A1(I)
      WRITE BINAPY (III) A2
      LL=LL+1
6    CONTINUE
1    CONTINUE
      CALL FCLOS (III)
      III=III+1
      TYPE 'LEVEL',M
10   CONTINUE
      CALL FCHAN ('TEST2.SV')
      END

```

```

      SUBROUTINE EIGEN(A,R,N,MV)
      DIMENSION A(1),R(1)
5      FANGE=1.0E-6
      IF(MV-1) 10,25,10
10     IQ=-N
      DO 20 J=1,N
      IQ=IQ+N
      DO 20 I=1,N
      IJ=IQ+I
      R(IJ)=0.0
      IF(I-J) 20,15,20
15     R(IJ)=1.0
20     CONTINUE
25     ANORM=0.0
      DO 35 I=1,N
      DO 35 J=1,N
      IF(I-J) 30,35,30
30     IA=I+(J+J-J)/2
      ANORM=ANORM+A(IA)*A(IA)
35     CONTINUE
      IF(ANORM) 165,165,40
40     ANORM=1.414*SQRT(ANORM)
      ANFMX=ANORM*RANGE/FLOAT(N)
      IND=0
      THR=ANORM
45     THR=THR/FLOAT(N)
50     L=1
55     M=L+1
60     MQ=(M*M-M)/2
      LQ=(L*L-L)/2
      LM=L+MQ
62     IF(ABS(A(LM))-THR) 130,65,65
65     IND=1
      LL=L+LQ
      MM=M+MQ
      X=0.5*(A(LL)-A(MM))
68     Y=-A(LM)/SQRT(A(LM)*A(LM)+X*X)
      IF(X) 70,75,75
70     Y=-Y
75     SINX=Y/SQRT(2.0*(1.0+(SQRT(1.0-Y*Y))))
      SINX2=SINX*SINX
78     COSX=SQRT(1.0-SINX2)
      COSX2=COSX*COSX
      SINCS=SINX*COSX
      ILC=N*(L-1)
      IMQ=N*(M-1)

```

```

      DO 125 I=1,N
      IC=(I*I-I)/2
      IF(I-L) 80,115,80
80    IF(I-M) 85,115,90
85    IM=I+MQ
      GO TO 95
90    IM=M+IC
      95    IF(I-L) 100,105,105
100   IL=I+LQ
      GO TO 110
105   IL=L+IQ
110   X=A(IL)*COSX-A(IM)*SINX
      A(IM)=A(IL)*SINX+A(IM)*COSX
      A(IL)=X
115   IF(MV-1) 120,125,120
120   ILR=ILQ+I
      IMR=IMQ+I
      X=R(ILR)*COSX-R(IMR)*SINX
      R(IMR)=R(ILR)*SINX+R(IMR)*COSX
      R(ILR)=X
125   CONTINUE
      X=2.0*A(LM)*SINCS
      Y=A(LL)*COSX2+A(MM)*SINX2-X
      X=A(LL)*SINX2+A(MM)*COSX2+X
      A(LM)=(A(LL)-A(MM))*SINCS+A(LM)*(COSX2-SINX2)
      A(LL)=Y
      A(MM)=X
130   IF(M-N) 135,140,135
135   M=M+1
      GO TO 60
140   IF(L-(N-1)) 145,150,145
145   L=L+1
      GO TO 55
150   IF(IND-1) 160,155,160
155   IND=0
      GO TO 50
160   IF(THR-ANRMX) 165,165,45
165   IC=-N
      DO 185 I=1,N
      IC=IC+N
      LL=I+(I*I-I)/2
      JG=N*(I-2)
      DO 185 J=1,N
      JG=JG+N
      MM=J+(J*J-J)/2
      IF(A(LL)-A(MM)) 170,185,185
170   X=A(LL)
      A(LL)=A(MM)
      A(MM)=X
      IF(MV-1) 175,185,175
175   DO 180 K=1,N
      ILR=IC+K

```

```
      IMF=JG+K  
      X=F(ILF)  
      F(ILF)=F(IMR)  
180    R(IMR)=X  
185    CONTINUE  
      PETURN  
      END
```

F

```

DIMENSION FINT(400)
COMMON FINT,TEM
TYPE 'TEST2'
CALL RESET
CALL FOPEN(0,'A000',4)
CALL FOPEN(1,'A100',4)
CALL FOPEN(2,'A010',4)
CALL FOPEN(3,'A110',4)
CALL FOPEN (4,'A020',4)
CALL FOPEN (5,'A120',4)
L=25
LN=L+1+(L)*(L+1)
EL1=3657.054
EL11=EL1
EL2=5225.0-1590.0
EL21=EL2
EL3=6761.0-3151.0
EL31=EL3
DO 11 IJ=2,LN
CALL FSEEK (1,IJ)
READ BINARY (1) A2
A22=A2
CALL FSEEK (0,IJ)
READ BINARY (0) A2
EL1=A22-A2+EL11
CALL FSEEK (1,IJ)
WRITE BINARY (1) EL1
CALL FSEEK (3,IJ)
READ BINARY (3) A2
A23=A2
CALL FSEEK (2,IJ)
READ BINARY (2) A2
EL2=A23-A2+EL21
CALL FSEEK (3,IJ)
WRITE BINARY (3) EL2
CALL FSEEK (5,IJ)
READ BINARY (5) A2
A24=A2
CALL FSEEK (4,IJ)
READ BINARY (4) A2
EL3=A24-A2+EL31
CALL FSEEK (5,IJ)
WRITE BINARY (5) EL3

```

```

11      CONTINUE
        CALL FSEEK (1,1)
        WRITE BINARY (1) EL11
        CALL FSEEK (3,1)
        WRITE BINARY (3) EL21
        CALL FSEEK (5,1)
        WRITE BINARY (5) EL31
C      THE REMAINDER OF THE PROGRAM CALCULATES THE
C      LINE INTENSITIES AND CONVOLUTES THE LINE
C      SPECTRUM INTO AN INSTRUMENT SPECTRUM
C      WITH A TRIANGULAR SLIT FUNCTION USING A
C      BANDWIDTH OF 8 WAVE-NUMBERS FOR VARIOUS
C      TEMPERATURES
C      I(J) IS PROPORTIONAL TO 2(J+1)G EXP(-(EROT+EVIB)/KT)
C
        CONST=(6.62559E-27*3.0E10)/(1.38054E-16)
        TEM=1500.0
        EL11=0.0
        EL21=1590.0
        EL31=3151.0
        EXP11=EXP(-(EL11)*CONST/TEM)
        EXP21=EXP(-(EL21)*CONST/TEM)
        EXP31=EXP(-(EL31)*CONST/TEM)
        DO 12 IJ=2, LN
          CALL FSEEK (0,IJ)
          READ BINARY (0) A2
          A22=A2
          CALL FSEEK (2,IJ)
          READ BINARY (2) A2
          A23=A2
          CALL FSEEK (4,IJ)
          READ BINARY (4) A2
          A24=A2
          EXP1=EXP(-(A22+EL11)*CONST/TEM)
          CALL FSEEK (0,IJ)
          WRITE BINARY (0) EXP1
          EXP2=EXP(-(A23+EL21)*CONST/TEM)
          CALL FSEEK (2,IJ)
          WRITE BINARY (2) EXP2
          EXP3=EXP(-(A24+EL31)*CONST/TEM)
          CALL FSEEK (4,IJ)
          WRITE BINARY (4) EXP3
12      CONTINUE
        CALL FSEEK (0,1)
        WRITE BINARY (0) EXP11
        CALL FSEEK (2,1)
        WRITE BINARY (2) EXP21
        CALL FSEEK (4,1)
        WRITE BINARY (4) EXP31
        N=0
        K=1

```



```

      LI=L+1
      CALL FSEEK (0,1)
      CALL FSEEK (2,1)
      CALL FSEEK (4,1)
      DO 13 J=1,LI
      JJ=(2*J)-1
      DO 22 I=1,JJ
      READ BINARY (0) EXP1
      EXPJ1=EXP1*((2*N)+1)
      CALL FSEEK (0,K)
      WRITE BINARY (0) EXPJ1
      READ BINARY (2) EXP2
      EXPJ2=EXP2*((2*N)+1)
      CALL FSEEK (2,K)
      WRITE BINARY (2) EXPJ2
      READ BINARY (4) EXP3
      EXPJ3=EXP3*((2*N)+1)
      CALL FSEEK (4,K)
      WRITE BINARY (4) EXPJ3
      K=K+1
22    CONTINUE
      N=N+J
13    CONTINUE
      LI=L+1
      CALL FSEEK (0,1)
      CALL FSEEK (2,1)
      CALL FSEEK (4,1)
      K=1
      G=3.0
      G1=1.0
      DO 14 J=1,LI
      JJ=(2*J)-1
      DO 23 I=1,JJ
      READ BINARY (0) EXPJ1
      TENS1=EXPJ1*G
      CALL FSEEK (0,K)
      WRITE BINARY (0) TENS1
      READ BINARY (2) EXPJ2
      TENS2=EXPJ2*G1
      CALL FSEEK (2,K)
      WRITE BINARY (2) TENS2
      READ BINARY (4) EXPJ3
      TENS3=EXPJ3*G
      CALL FSEEK (4,K)
      WRITE BINARY (4) TENS3
      JI=J-1
      IF(I.NE.JI) GO TO 230
      GG=G
      G=G1
      G1=GG
230   K=K+1
23    CONTINUE
14    CONTINUE
      CALL FCHAN ('TEST3.SV')
      END

```

C
C
C

CONVOLUTION STEP FOR 3500-3700 WAVE-NUMBERS REGION

```

DIMENSION FINT(450) , AEL1(700), AEL2(700), AEL3(700)
DIMENSION ATENS1(700), ATENS2(700), ATENS3(700)
COMMON FINT, TEM
TYPE 'TEST3'
CALL FOPEN (0, 'A000', 4)
CALL FOPEN (1, 'A100', 4)
CALL FOPEN (2, 'A010', 4)
CALL FOPEN (3, 'A110', 4)
CALL FOPEN (4, 'A020', 4)
CALL FOPEN (5, 'A120', 4)
L=25
LN=L+1+(L)*(L+1)
CALL FSEEK (0, 1)
CALL FSEEK (1, 1)
CALL FSEEK (2, 1)
CALL FSEEK (3, 1)
CALL FSEEK (4, 1)
CALL FSEEK (5, 1)
DO 1 I=1, LN
  READ BINARY (0) TENS1
  READ BINARY (1) EL1
  READ BINARY (2) TENS2
  READ BINARY (3) EL2
  READ BINARY (4) TENS3
  READ BINARY (5) EL3
  AEL1(I)=EL1
  AEL2(I)=EL2
  AEL3(I)=EL3
  ATENS1(I)=TENS1
  ATENS2(I)=TENS2
  ATENS3(I)=TENS3
1  CONTINUE
CONST=1.4397822
AREA=0.0
DO 40 I=1, LN
40  AREA=AREA+ATENS1(I)+ATENS2(I)+ATENS3(I)
DO 41 I=1, LN
  ATENS1(I)=ATENS1(I)/AREA
  ATENS2(I)=ATENS2(I)/AREA
41  ATENS3(I)=ATENS3(I)/AREA
INC=450
DO 23 I=1, INC
23  FINT(I)=0.0
MIN=3500
MAX=3700

```

```

      SW=8.
      FW=2*SW
      DO 25 K=1, LN
      KEL1=AEL1(K)
      KEL2=AEL2(K)
      KEL3=AEL3(K)
      I=(KEL1-MIN)*2
      II=(KEL2-MIN)*2
      III=(KEL3-MIN)*2
      IF(I.GT.416.OR.I.LT.-16)GO TO 28
      LM=-16
      DO 26 ILM=LM, 16
      WT1=ATENS1(K)*(FW-IABS(ILM))/FW
      IF(WT1.LE.0.0)GO TO 26
      M=I+ILM
      IF(M.LE.0)GO TO 26
      FINT(M)=FINT(M)+WT1
26      CONTINUE
28      IF(II.GT.416.OR.II.LT.-16)GO TO 29
      LM=-16
      DO 27 ILM=LM, 16
      WT2=ATENS2(K)*(FW-IABS(ILM))/FW
      IF(WT2.LE.0.0)GO TO 27
      M=II+ILM
      IF(M.LE.0)GO TO 27
      FINT(M)=FINT(M)+WT2
27      CONTINUE
29      IF(III.GT.416.OR.III.LT.0)GO TO 25
      LM=-16
      DO 30 ILM=LM, 16
      WT3=ATENS3(K)*(FW-IABS(ILM))/FW
      IF(WT3.LE.0.0)GO TO 30
      M=III+ILM
      IF(M.LE.0.0)GO TO 30
      FINT(M)=FINT(M)+WT3
30      CONTINUE
25      CONTINUE
      ANORM=.612553
      DO 401 I=1, 400
401      FINT(I)=FINT(I)/ANORM
      CALL FCHAN ('TEST4.SV')
      END

```

R

```

C      TITLE FOR A SPECIFIC TEMPERATURE
C
      DIMENSION LEL1(8),LEL2(10),IHOL(9),LHOL(12)
      DIMENSION FINT (450)
      COMMON/LE/LEL1,LEL2,IHOL,LHOL
      COMMON FINT,TEM
      DATA LEL1/'FREQUENCY CM-1'/
      DATA LEL2/'RELATIVE INTENSITY'/
      DATA IHOL/'TEMPERATURE (K)'/
      DATA LHOL/'PAMAN SPECTRUM OF H2O '/
      TYPE 'TEST4'
      YY=0.0
      XX=0.0
      FLTX=3500.0
      FLTY=0.0
      CALL INITAL (6,200,11.0,17.0)
      CALL PLOT (0.5,1.2,-3)
      CALL PLOT (0.0,0.0,0)
      CALL AXIS (0.0,0.0,LEL1,-14,10.0,0.0,3500.0,20.0,1)
      CALL AXIS (0.0,0.0,LEL2,18,5.0,90.0,0.0,0.2,1)
      CALL NUMBER (0.5,6.0,.21,TEM,0.0,0)
      CALL SYMBOL (4.0,6.0,.21,IHOL,0.0,15)
      CALL SYMBOL (0.5,7.0,.21,LHOL,0.0,22)
      X=0.0
      CALL PLOT (0.0,0.0,3)
      CALL PENEN
      DO 73 I=1,400
      Y=FINT(I)*5.0
      CALL PLOT (X,Y,1)
73    X=X+0.025
      CALL PENUP
      CALL FSTP
      CALL FESET
100  STOP
      END
F.

```